FACULDADE DE ENGENHARIA DA UNIVERSIDADE DO PORTO

Computational Study on the Dorsolumbar Compression Fracture and its Fixation Methods

Ana Rita Reis

DISSERTATION

INTEGRATED MASTER IN BIOENGINEERING

Supervisor: Marco Parente

Co-supervisor: Luisa Sousa

April 19, 2021

Resumo

A coluna vertebral suporta grande parte da carga do corpo e é a grande responsável pela mobilidade do mesmo. Pelo menos uma vez na vida, uma pessoa sente dores na zona dorsolombar, já que é neste local que reside a transição da zona torácica para a lombar e onde é exercida a maior parte da força.

O presente caso de estudo contempla as fraturas traumáticas vertebrais (com origem em queda), que resultaram da exposição a uma grande força axial, mais especificamente as de compressão do tipo A4 - *complete burst*.

Uma vez que este tipo de fratura pode levar a problemas neurológicos, é necessário o tratamento via cirúrgica. Foram então propostos, a estudo, dois tratamentos cirúrgicos para a fratura na vértebra L1: *fixação posterior de segmento curto com a adição de parafusos intermédios* e *fixação posterior de segmento longo*. Tal como o nome indica, as diferenças estão no número de vértebras usadas no procedimento e na utilização ou não da vértebra fraturada. No primeiro tratamento são utilizados parafusos na vértebra T12, L1 (fraturada) e L2. No segundo, apenas as vértebras T11, T12, L2 e L3 são aparafusadas. Assim, é necessário perceber o comportamento biomecânico tanto da coluna saudável, como do seu comportamento após a execução de cada tratamento.

O objetivo da presente dissertação é a compraração do comportamento biomecânico dos dois métodos de fixação posterior da coluna dorsolombar referidos. Para tal, através do método de elementos finitos, criaram-se primeiramente os modelos saudáveis e patológico com a fratura de tipo A4 na vértebra L1, seguidos dos modelos propostos. Nestes foram consideradas as vértebras desde a T11 à L1, os seus discos intervertebrais, ligamentos, barras e parafusos de fixação. Recriou-se as condições fronteira, interações e aplicou-se um momento de 5 Nm.

Para cada unidade funcional de todos os modelos foi calculado a amplitude do movimento (ROM). Posteriormente os resultados dos dois modelos de fixação foram comparados, nomeadamente os deslocamentos máximos.

Verificou-se que o modelo de *fixação posterior de segmento longo* atribui uma maior rigidez ao segmento da coluna vertebral. Concluiu-se assim, que este é o melhor método para a fixação posterior da coluna dorsolombar com uma fratura de tipo A4, quando comparado com o modelo de *fixação posterior de segmento curto com a adição de parafusos intermédios*.

Palavras chave: biomecânica; coluna vertebral; dorsolombar; fratura de explosão completa; fixação posterior de segmento curto com a adição de parafusos intermédios; fixação posterior de segmento longo.

Abstract

The vertebral column supports the main body weight, and it is responsible for its mobility. Once in a lifetime, dorsolumbar pain is felt since it is the spot where the transaction between the thoracic and lumbar areas occurs, and most of the major forces are applied.

This case study embraces the traumatic vertebral fractures (with fall origin), resulting from exposure to high axial forces, specifically to compression fractures of type A4 - complete burst.

As this type of fracture can lead to neurological problems, surgical treatment is necessary. Therefore, two surgical treatments for the L1 fracture were proposed: *Posterior Short Segment Fixation with Intermediate Screws* and *Posterior Long Segment Fixation*. As suggested, the main differences are in the number of vertebrae used during the procedure and the use of the injured vertebra. In the first treatment, vertebra T12, L1 (injured) and L2 are screwed. On the other hand, T11, T12, L2, and L3 are screwed in the second one. Nevertheless, it is necessary to understand the biomechanical behaviour both of the healthy column and its post treatment one.

The goal of the present dissertation is the biomechanical comparison between the two posterior fixation models of the dorsolumbar column through computational study. Such was achieved by creating both models with 3D finite element method after the healthy and complete burst models. That consisted of the vertebrae from T11 to L3, the respective intervertebral discs, ligaments and the fixation apparatus (screws and rods). The boundary conditions were simulated and a load of 5 Nm was applied.

It was calculated each models' functional units ROM. Posteriorly both fixation models' results were compared with the intact and complete burst in order to be compared with one another. The total displacement was obtained as well.

It was verified that the *Posterior Long Segment Fixation* results in a greater segmental stiffness. In conclusion, this technique shows to be the best approach for the posterior dorsolumbar fixation for the complete burst fracture, when compared with the *Posterior Short Segment Fixation with Intermediate Screws*.

Keywords: biomechanics; complete burst; dorsolumbar; Posterior Long Segment Fixation; Posterior Short Segment Fixation with Intermediate Screws; vertebral column.

Agradecimentos

Estando a terminar o meu percurso académico do Mestrado Integrado em Bioengenharia (MIB), cabe-me agradecer a quem tornou possível o sentimento de realização durante estes anos. Desde a ajuda motivacional à ajuda de superação de todas as etapas que até aqui me trouxeram.

Agradeço ao meu orientador, o Professor Doutor Marco Parente, por todo o conhecimento e paixão que me deu pela àrea da biomecânica, por todo o apoio dado e por conseguir salvar as minhas simulações quando já havia chegado a um impasse durante este último ano.

Agradeço também à minha coorintadora, a Professora Doutora Luisa Sousa, sem ela esta dissertação não seria possível. Agradeço por toda a preocupação e disponibilidade tida durante este ano.

Agradeço ao Professor Bruno Areias por ter dado a sua valiosa ajuda durante esta dissertação, quer na introdução aos programas *Meshmixer* e *Rhinoceros* como na constante disponibilidade e paciência para ajudar na resolução de problemas nas morosas simulações, explicando sempre a teoria por detrás de cada um.

Gostaria de agradecer ao Doutor Maia Gongalves pela proposta da presente dissertação, por todo o apoio durante a execução da mesma e por ter sido uma grande ponte entre a ortopedia e a biomecânica, estando sempre disposto a tirar qualquer dúvida da sua àrea.

Agradeço ao Doutor Henrique Sousa por fazer parte deste projeto e validar algumas questões referentes à anatomia da coluna vertebral.

Agradeço às faculdades que fizeram parte do meu percurso, UTAD e FEUP, não só aos professores por me darem conhecimento e ferramentas provenientes do curso de Bioengenhaia, como também a todas as atividades extra curriculares que permitiram desenvolver capacidades e criar laços com amigos desde caloira, a Tina, a Catarina, o Bogas, o Nuno e a Madalena, sem eles estes anos não teriam tido o mesmo brilho. Agradeço também ao BEST Porto, em especial à Mariana, Margarida, Rui e Afonso, agradeço todas as palavras de carinho, todas as conversas de reflexão e mesmo na ajuda no curso tanto durante o tempo de direção como nos dias de hoje.

Agradeço às minhas amigas já de longa data, a Rita Moreira e a Ana Castro por todos os momentos passados e por crescerem comigo.

Agradeço ao meu namorado Alberto Santos que acompanhou esta etapa de perto, desde os altos aos baixos, e nunca me deixou desistir, levando-me a fazer mais e melhor. Agradeço-lhe todos os momentos de carinho, por alimentar a minha curiosidade e vice-versa. E por todos os dias me tornar numa pessoa melhor, mais curiosa e sobretudo mais completa.

Em último, mas nunca menos importante, quero agradecer à minha família quer estejam perto ou longe, ou a quem já não está, cuidaram e cuidam diariamente de mim. Agradecer não chega por toda a educação que me deram e por acreditarem sempre em mim. Sobretudo os meus pais que fizeram sacrifícios para me conseguirem proporcionar a melhor educação, deixaram-me errar estando sempre ao meu lado, mostraram-me que é preciso trabalhar para os meus sonhos e ao mesmo tempo nunca deixar de ser humilde. Eles são a minha maior inspiração e só assim consigo chegar mais longe.

Contents

List of Figures

List of Tables

Abbreviations

3D	Three Dimensional
ALL	Anterior Longitudinal Ligament
C	Cervical
CL	Capsular Ligament
CT	Computerized Tomography
FE	Finite Element
FEM	Finite Element Method
IAR	Instantaneous Axis of Rotation
ISL	Interspinous Ligament
L	Lumbar
LBP	Low Back Pain
LF	Ligament Flavum
MRI	Magnetic Resonance Imaging
N/A	Not Applicable
PL	Posterior Long Segment Fixation
PLL	Posterior Longitudinal Ligament
PSS	Posterior Short Segment Fixation with Intermediate Screws
ROM	Range of Motion
SSL	Supraspinous Ligament
T	Thoracic

Chapter 1

Introduction

This chapter addresses a broad context on the low back pain issue, along the lines of introducing alternative surgical treatments that led to the motivation of the present dissertation. It is also shown its purpose and the structure of this document.

1.1 Context

Low back pain (LPB) can be characterized as an ache in the lumbar portion of the spine, which ranges from a slight build-up pain to sudden and intense one. LBP is classified by its duration as acute, sub-acute or chronic, *i.e.*, pain lasting less than 6 weeks, 6 to 12 weeks or more than 12 weeks, respectively. Since the low back discomfort and pain have many origins, the scope of people that suffer from this symptom goes from young to elderly, and its prevalence rate can go from 4% to 69%, according to different studies' parameters it is directly proportional to the age. Thus, LBP is one of the largest causes of a musculoskeletal disability [1].

Sudden movements or poor body mechanics while lifting heavy objects can lead to muscle sprains or strains. A fall can lead to spine fractures, whether on healthy or diseased bone. These are some examples that prompt low back pain, hence the diagnostic of the injury needs to have into consideration some clinical history aspects, combined with specific physical assessments. If the doctor suspects of a certain condition, a diagnostic imaging test is made, a CT (Computerized Tomography) scan or an MRI (Magnetic Resonance Imaging).

A proper diagnostic is essential to best identify the right treatment. Sometimes when rest, medication and therapy don't work within some weeks, surgery is the best option to relief the pain. In this case, the patient must be aware of the risks, advantages and disadvantages of the procedure, in the long and short term.

1.2 Motivation

Spine surgery can come along with some serious complications during and after the procedure, such as subsequent pain, loss of mobility, prosthesis's displacement and the need for additional surgery. The spine's biomechanics study must ally with the technology evolution that we are facing in order to avoid or minimise such risks.

Through structures' modelling and reality-based biomechanics' numerical simulation using finite element methods (FEM), it is possible to estimate the position of an implant after several loads applied with motion, as well as the rupture point of the biomaterial, the bone tissues and those nearby. The use of this method to understan the behaviour of the human spinal column was initiated by Liu and Ray in 1973 [2]. Since then, there have been many FEM applications to the human low back.

Nowadays, regarding the medicine field, biomechanics is fully present in orthopaedics [3], in which a specific problem is solved with numerical simulation and further parameter identification of the previous.

1.3 Goals

The present dissertation in regards to *Computational Study on the Dorsolumbar Compression Fracture and its Fixation Methods* has the purpose of aiding the decision making of spine surgeons when finding the most sturdy treatment for a level A4 fracture of the L1 vertebra (or similar).

Before reaching any goal, there's the grasping requirement for the pathology at stake, the A4 fracture of the L1 vertebra's body, caused by compression. Therefore, a theoretical approach of the biomechanic behaviour between vertebra and their discs is needed, as well as the exploration of the disease treatment, both fixation methods included.

In order to achieve the main goal of finding the best fixation method, *posterior short segment fixation with intermediate screws* or *posterior long segment fixation*, by mechanical behaviour comparison, some previous steps must be carried.

With the aim of undertaking the numeric study of the previous, a mesh must be implemented to the modulated relevant structures of the dorso-lumbar spine and the implants from the surgical methods in question.

Finally, some loads interrelated with motions need to be applied to both models, on biomechanic simulators. For this purpose, their validation parameters are retrieved from reliable data.

1.4 Structure

This document is divided into five chapters.

The chapter 2 frames the problem covered in this work by a literature review. This has got a far-reaching on many matters related to the problem in order to fully apprehend the concepts of the spine's anatomy.

Further, the chapter 3 refers to basic principles of spinal biomechanics, which leads to a better understanding of the spinal pathologies also covered in this chapter. It which also includes statistics (incidence and prevalence) of the compression fracture of L1, how the surgical treatments are performed (*posterior short segment fixation with intermediate screws* and *posterior long segment fixation*), describing their pros and cons and some results.

The chapter 4 can be divided into four sections. The first is the FE modulation of the intact T11-L3 model, the second is the modelling of the complete burst fracture (on L1 vertebra) model, the third is the modelling of the posterior short segment fixation with intermediate screws and the fourth and final, the modelling of posterior long segment fixation model. Each contains the steps taken, i.e., components FE modelling, their mechanical properties, contact conditions between them, boundary conditions and finally, the loads applied.

According to the chapter 4 developed models, each one was submitted for results which can be found in chapter 5. These contain the validation of the intact model, the model with the pathology and the two treatments results.

Lastly, the chapter 6 summarizes all the preceding chapters with some final reflections, as well as a future work recap, by giving some final considerations.

Chapter 2

Spinal Literature Review

The vertebral spine is present not only in humans but also in other vertebral animal species. Its geneses in amniotes differ from the anamniotes from the early beginning of their formation [4]. Considering all the different paths of cells' differentiation into a fully developed spine in both amniotes and anamniotes, and all their subdivisions, this chapter it will only focus on the Human vertebral spine and all the surrounding elements, necessary for giving it structure and functionality.

2.1 Spinal Embryology Overview

Regarding the anatomy of a fully developed spine, its origins must be taken into consideration with the purpose of better understanding its structure and its purpose.

In the early embryonic development, as seen in figure 2.1 the embryo from the second week of gestational age is formed by the endoderm, the epiblast and the mesoderm [5]. After the corresponding folds are formed, during the neurulation, the last one gets divided into axial mesoderm, which gives rise to the notochordal process, and later becomes the notochord; lateral plate at the periphery; paraxial mesoderm, also known as presomitic mesoderm, since it will give rise to the somites, and lying adjacent to the notochord, on either side of it; and intermediate mesoderm between the two.

Every level of spine growth is distinct from the subsequent one, making it a complex process. Despite the different rate of the component formation, they are perfectly in synchrony. The migration of somites and the differentiation of sclerotomes, which are organized around the notochord, define the first two months of the embryo.

Two hemisomites from different structures give rise to a vertebra, it should be noted that each somite is divided into two hemisomites. The caudal end of each somite fuses with the cephalic end of the underlying somite, here the precursor of the vertebra is formed. Along these lines, eight cervical somites with eight corresponding nerve roots will generate seven cervical vertebrae.

It is known that between two vertebrae there is a disc. The annulus fibrosus of the intervertebral disc is formed from the cells of the sclerotome. The notochord will disappear gradually, and its remnants will form the nucleus pulposus [6].

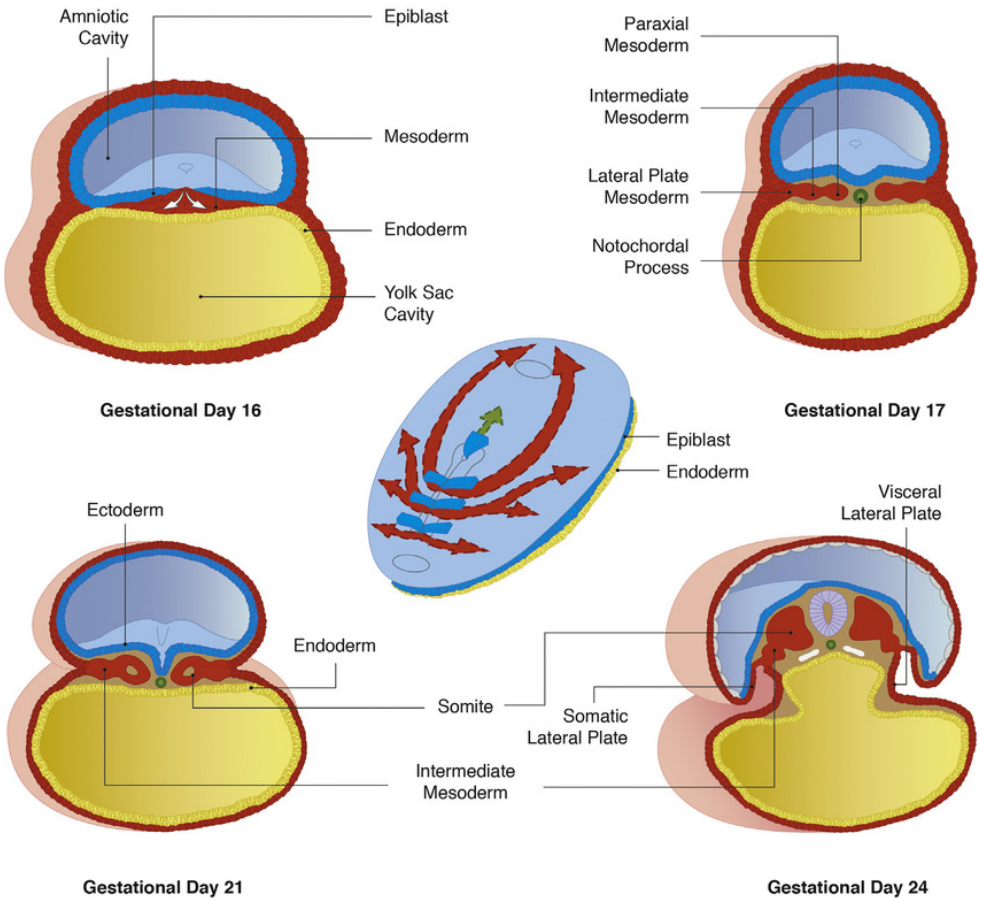

Figure 2.1: Illustration of the formation of Mesoderm.

Cells of the sclerotomes also migrate around the neural tube and fuse dorsally, creating the vertebral arch, which has the function of protecting the spinal cord [7].

Finally, the ossification of the vertebrae can be divided into three primary centres and five secondary centres. In the centrum is located one primary centre, the other two are on each side on the neural processes. The tip of the spinous process, the tip of both transverse processes, and the superior and inferior surfaces of the vertebral body are the secondary ossification centres [8].

Summarizing, there are three main periods that lead to the growth of the spine:

1. The embryonic period, which the vertebral envelope and the cord are formed;

2. The fetal period that corresponds to the beginning of vertebral ossification;

3. The postnatal period, which is characterized by progression in ossification and decisive phases, especially in the first 5 years of life.

2.2 Spinal Anatomy Overview

The spine, also known as the vertebral column or backbone, consists in a total of 33 bones : 7 cervical vertebrae, 12 thoracic vertebrae, 5 lumbar vertebrae, 5 sacral vertebrae, and 4 coccygeal vertebrae [9], in an embryo. However, in its full form, the mentioned five sacral vertebrae are merged, the same happens to the coccygeal vertebrae. These combined with the skull, ribs, and sternum create the axial skeletal system.

Figure 2.2 ([10]) illustrates five different regions of the vertebral column in the anterior, posterior and lateral views (from left to right). From top to bottom, the first set is the cervical (C1-C7), followed by the thoracic vertebrae (T1-T12), the lumbar (L1-L5), the sacrum, and, finally, the coccyx, all together represent 40% of full body height [11].

2.2.1 The Spine Main Function

As a generic function, vertebral column gives structural support to humans, as well as protect neurons as they carry information to and from the brain [8].

The principal mechanical functions of the vertebral column can be divided into five [12, 13]:

1. It is the torso and head weight support;
2. It gives protection to the spinal cord, as it contains the spinal cord within the vertebral canal, and nerve roots;
3. It allows the nerves exit the spine;
4. It is the muscle connection local;
5. It also provides head movement as well as movement for flexibility and locomotion, as it has articulations, ligaments, and muscles.

The protection of the spinal cord and spinal nerves can be explained since the spinal cord it is inside the spinal canal, which is created by the central lumen of each vertebral body. At each vertebral level, spinal nerves emerge from the main cord. The diameter of the spinal canal changes in the different parts of the vertebral column, larger in the cervical and lumbar regions and smaller in the thoracic region.

The spine forms the central axis of weight-bearing and supports the head as well as transfers the weight of the trunk and abdomen to the legs [9], providing the function of structural support.

It also provides structure and flexibility to the body with the help of all the vertebral motion segments through the spine, which allows rotation and bending. The cushioning between the vertebrae is provided by the intervertebral discs. In the thoracic region, the structure is given by the attachment of the ribs in the their proper sites. It also serves as the attachment site for multiple muscles.

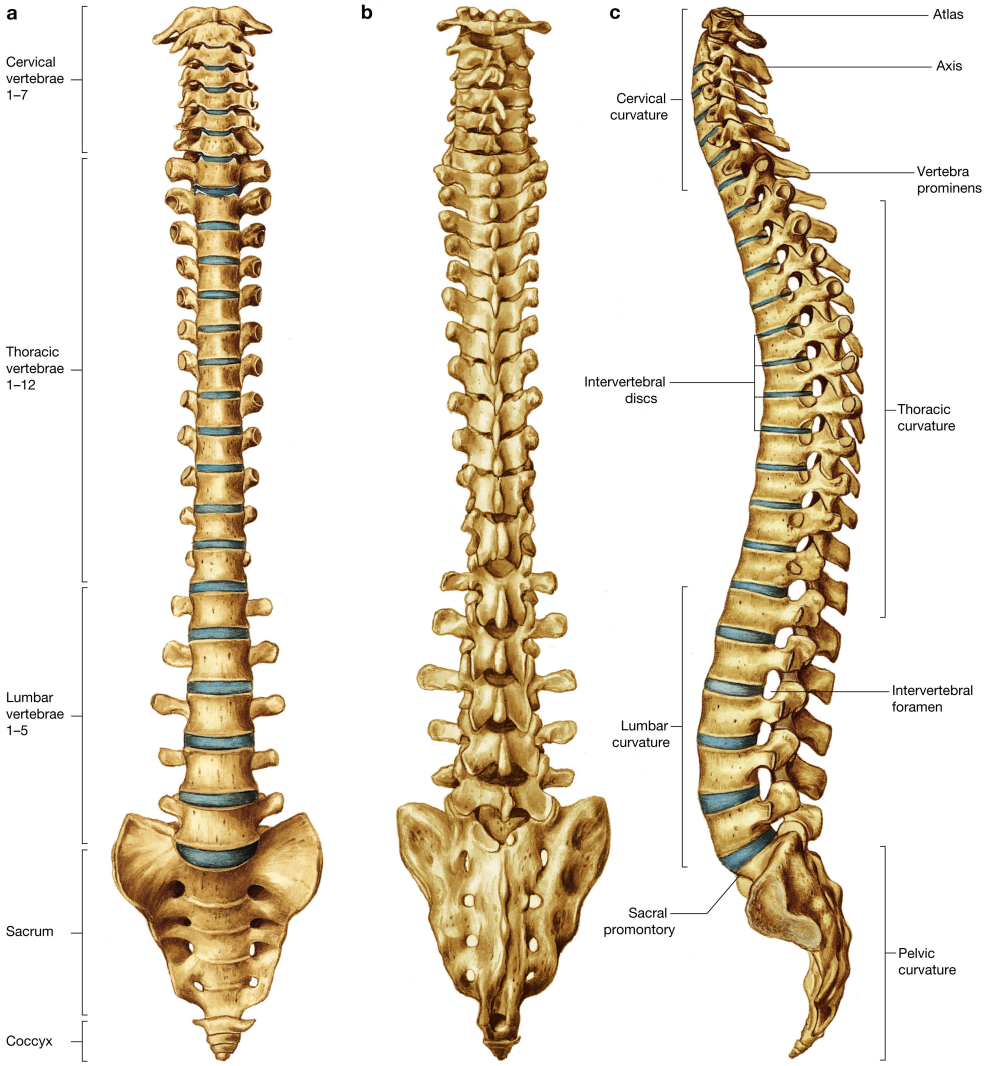

Figure 2.2: Illustration of the anterior, posterior and lateral views (from left to right) of a articulated vertebral column in an adult.

2.2.2 The Spine Curvature

In the fetus, the vertebral column is curved in the shape of the letter C (concave ventrally and reciprocally convex dorsally).

This anterior concavity is termed the primary curvature of the vertebral column, and this kyphosis is retained throughout life in the thoracic, sacrococcygeal (sacral and coccygeal) regions of the column.

After birth, during the infancy, secondary curvatures with an anterior convexity (lordosis) appear gradually in the cervical and lumbar regions, resulting in the permanent sinuous curves of the fully developed spinal column that is evident when the column is shown in profile (Figure 2.3). The cervical lordosis is the consequence of the sustained extension of the head and neck produced

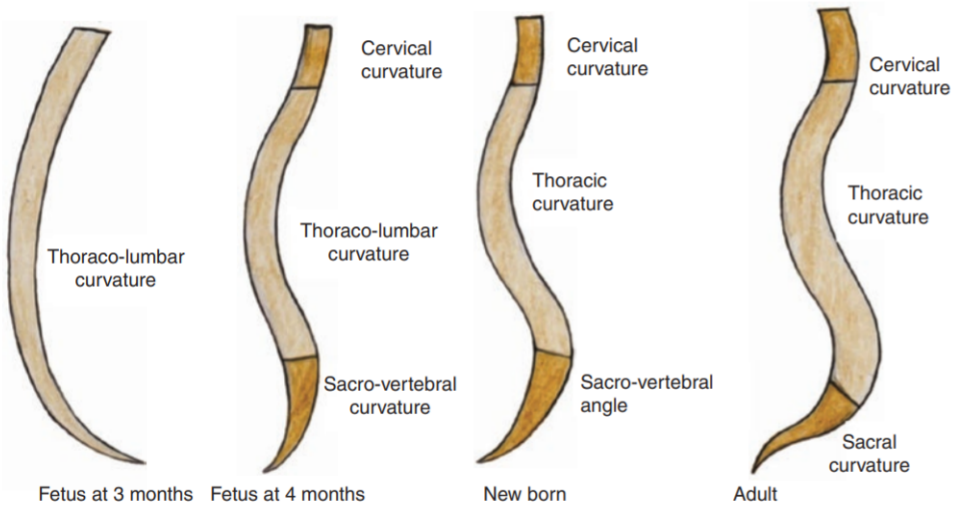

Figure 2.3: Illustration of the column's curvature evolution.

by the postvertebral muscles when the child first holds up its head. The lumbar lordosis appears much later and is associated with the muscular support of the trunk provided by the powerful postvertebral muscles when the infant begins to sit upright, stand, and walk [10, 13, 14].

In figure 2.3 [11] an illustration of Evolution of spinal curvatures is shown. From left to right, the fetus at 3 months has a large "C" curvature. At 4 months it is already notorious the appearance of the sacro-vertebral angle. From birth to 1 year (depending on child development) the holding of the head heralds the cervical lordosis, the holding of the trunk, the thoracic kyphosis and the vertical posture is accompanied by the lumbar curvature. At adult age, all the previous curvatures are even more prominent, as shown in figure 2.2, where the pelvic curvature represents the sacral and coccygeal curvature.

2.2.3 The Functional Spinal Unit

The structural and functional unit of the vertebral column is the vertebral motion segment, illustrated in figure 2.4 [10]. A vertebral motion segment consists of two adjoining vertebrae and interposed soft tissue structures, i.e., it is defined as any two successive, moveable vertebrae including the structures and articulations that unite them, from C2-C3 to L11-L12. The human vertebral column is the combination of all the functional spinal units and the sacrococcygeal complex.

Each vertebral motion segment can be divided into anterior portion and a posterior portion, regarding its function and morphology [15].

On one hand, the anterior portion of the vertebral motion segment is formed by two adjacent vertebral bodies and one intervertebral disc in between, and corresponding ligaments. It has the function of bearing and diffuse internal and external loads, that are 80% of the total of the standing loads.

On the other hand, the posterior portion supports only 20% of the orthostatic loads. Its main function is guiding the orientation and amplitude of the vertebral column's motion, this is related to its elements. The posterior portion is formed by the pedicles, lamina, processes and facet joints of two consecutive vertebrae (figure 2.4).

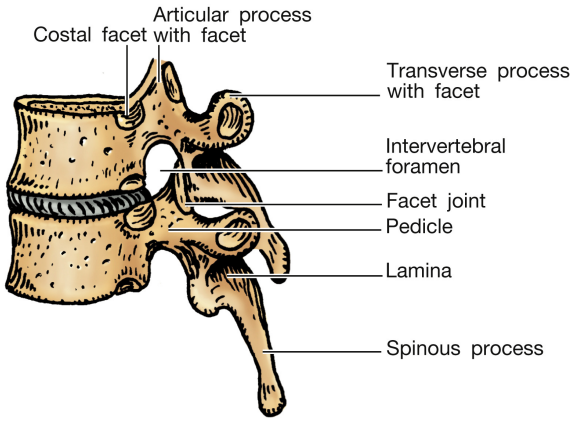

Figure 2.4: Illustration of a typical functional unit.

2.3 Vertebrae

2.3.1 Main Components

Vertebrae are irregular bones of the backbone. Each one is composed by two bone types: cancellous spongy bone, which forms the interior of the body and resembles scaffolds, due to its trabaculae (each trabecula consists of several lamellae with osteocytes between them) and cortical compact bone that covers the rest of the cancellous bone [16].

All the vertebrae, except C1 and C2, have the same typical elements, as shown in figure 2.5 [13]. Those are as follow:

1. **Body**: in a small length cylinder shape, with both flat surfaces in the superior and inferior directions. It is the weight-bearing portion of the vertebra. An intervertebral disc is located between two bodies;

2. **vertebral foramen**: The vertebral foramina of all the vertebrae form the vertebral canal, where the spinal cord is located;

3. **Vertebral arch**: forms the lateral and posterior walls of the vertebral foramen. It has articular surfaces and different processes;

4. **Pedicles**: extend from the body to the transverse process of each side of the vertebra

5. **Laminae**: extend from the transverse processes to the spinous process;

6. **Transverse processes**: It is also a local for muscle linkage;

7. **Spinous process**: projects dorsally from where the two laminae meet;

8. **Articular processes**: superior and inferior projections on each side. At their top sits a **articular facet** and in where the vertebrae articulate with each other.

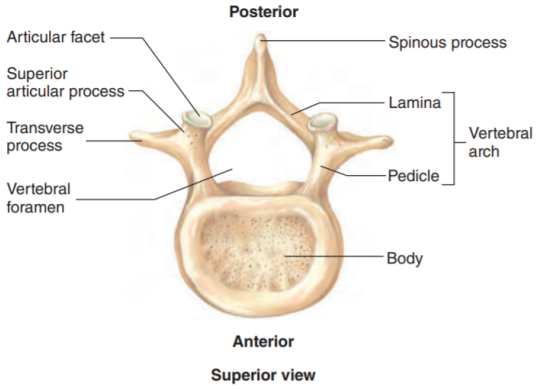

Figure 2.5: Illustration of a typical vertebra.

2.3.2 Regional Vertebrae Characteristics

There are no equal vertebrae. Despite their similarities as seen before, there are major differences that make each vertebra play a specific role in the vertebral column. In each region, the vertebrae have particular characteristics, which are described below.

1. **Cervical**

   The first cervical vertebra is called the Atlas, C1 (figure 2.6a [13]). The movement between the atlas and the occipital bone is responsible for a “yes” motion of the head. It also allows a slight tilting of the head from side to side. It is the only one without a body.

   The second cervical vertebra (2.6b) is called the axis, it is responsible for the "no" motion of the head, and its considerable rotation. This rotation occurs around The Dens process, which points superiorly from the axis.

   The six vertebrae (C1 excluded) have very small bodies (2.6b,c). Due to this characteristic, it is in the cervical region where the dislocations and fractures are more common.

   Each of the transverse processes has a transverse foramen (2.6c), which enables the vertebral arteries to pass towards the brain. An assorted amount of the cervical vertebrae also have partly split spinous processes [13, 17].

2. **Thoracic**

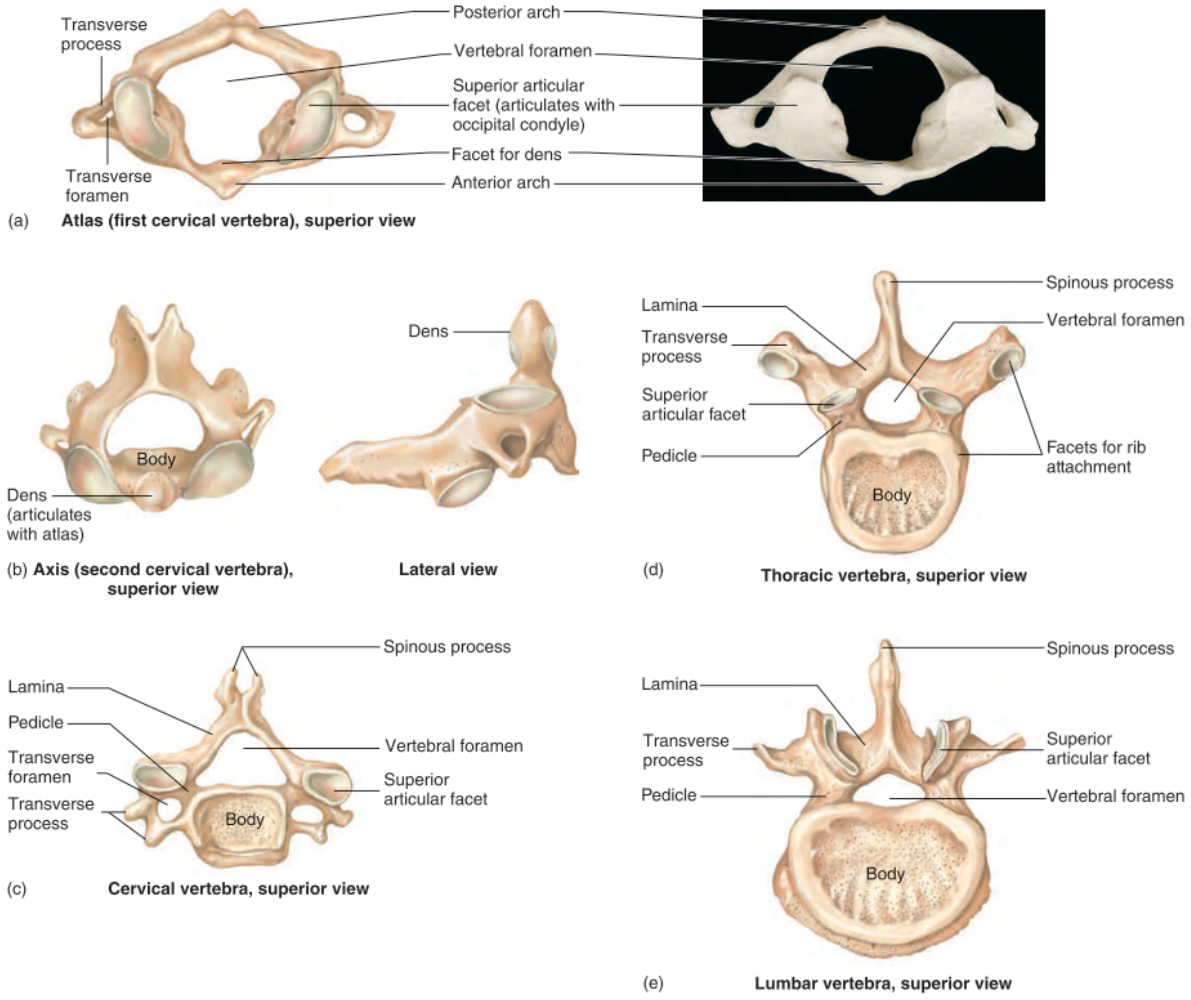

Figure 2.6: Illustration of the superior view of the first cervical vertebra, Atlas (a), the superior and lateral view of the second cervical vertebral (b), and the superior views of typical vertebrae, cervical (c), thoracic (d) and lumbar (e).

The 12 thoracic vertebrae (figure 2.6d) have long, thin spinous processes directed downwards. However, the last two or three thoracic vertebrae, have somewhat horizontal rather than sloping spinous processes. Also, they lack on articular facets on their transverse processes. The bodies of T5 to T8 vertebrae are flattened on their left sides due to their relationship with the descending thoracic aorta [10, 13, 17].

For each thoracic vertebra, there is a pair of ribs that is connected to the extra articular facets on their lateral surfaces (figure 2.6d). These can be divided into true ribs and false ribs. The true ribs, from 1 to 7, attach frontally to the sternum by means of costal cartilages. The false ribs, do not attach directly to the sternum, from 8–10 attach to the sternum by common cartilage, or do not attach at all, like ribs 11 and 12, for this matter of fact, they are called floating ribs [13].

3. **Lumbar**

   The lumbar vertebrae (L1-L5) (figure 2.6e) have bulky, rectangular transverse and spinous processes, and large, thick bodies, being the largest of the moveable vertebrae. Due to that characteristic, they carry a large amount of weight, leading to ruptured intervertebral discs, which does not happen as much in the other regions. The inferior articular facets face laterally, while the superior articular facets of the lumbar vertebrae face medially. This allows adjacent lumbar vertebrae to join together, giving more strength and stability to this region [10, 13, 17].

   All those attributes give the lumbar spine major functions. It helps to support the upper body. It also absorbs axial forces delivered from the head, neck, and trunk [18].

4. **Sacral**

   The five sacral vertebrae are fused into a single bone called the sacrum, as seen in figure 2.7 [13]). The spinous processes of the sacral vertebrae form the median sacral crest, except for the fifth, leaving a sacral hiatus at the inferior end of the sacrum. The sacral promontory is formed by the anterior edge of the body of the first sacral vertebra. Laterally, the sacrum articulates with the corresponding hip bone at the sacroiliac joint [10, 13, 17].

5. **Coccygeal**

   The column tailbone, or coccyx, consists of four fused vertebrae, visible at the end of the sacrum in figure 2.7. They atypical coccygeal vertebrae consist of extremely reduced vertebral bodies, without any foramina or processes, since they are fused into a single bone. During a fall by sitting down hard on a solid surface or during childbirth (women) the coccyx can be easily broben [13, 17].

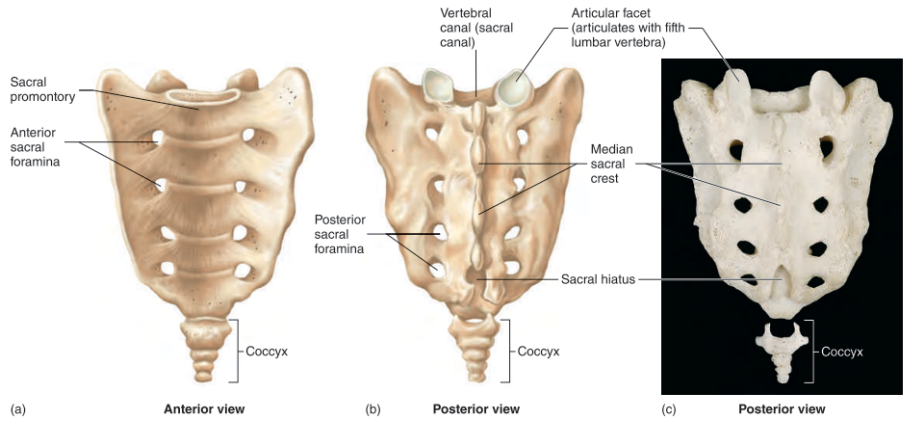

Figure 2.7: Illustration of the sacro-coccygel vertebral segment from an anterior view (a), posterior view (b). Posterior real anatomical view (c).

2.4 Intervertebral Discs

Intervertebral discs are cartilaginous structures located between two adjacent vertebrae composed three elements indicated below and exemplified in figure 2.8 [19]. Summing all of them, they make up 25% of the length of the vertebral column.

1. **annulus fibrosus**: composed mainly of collagenous fibres and has a laminated structure which surrounds the nucleus pulposus. The fibres of the lamellae are arranged obliquely in concentric rings that overlap one another (see figure 2.8). Its peripheral fibres insert into the endplates, and both anterior and posterior longitudinal ligaments.

2. **nucleus pulposus**: centrally located formed mainly of mucoid material, it contains 70% to 90% of water. From the moment that starts losing water throughout the years, the nucleus pulposus becomes less distinguishable from the annulus fibrosus.

3. **endplate**: it is considered cartilaginous and it is located between the vertebral body and disc. Behaves as a growth plate and transfuses nutrients from the vertebral body to the disc.

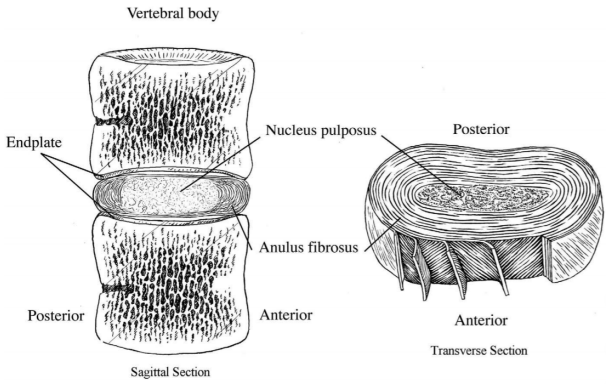

Figure 2.8: Illustration of the intervertrebal disc and its elements.

The nucleus pulposus and the annulus fibrosus of the intervertebral disc provide substantial resistance to axial stress, and support the anterior and posterior longitudinal ligaments, also noticeable in figure 2.9 [10]. The intervertebral disc also suffers from flexion, extension, and lateral bending forces, which can cause significant disc bulging and herniation. The disc lacks resistance to compression forces, whereas the angled orientation of the fibres of the annulus fibrosus (30° with the endplate) makes it effective at resisting rotation. disc bulging occurs on the concave side of a bending spine, leading to osteophyte formation. The nucleus pulposus moves in the opposite direction [9, 20].

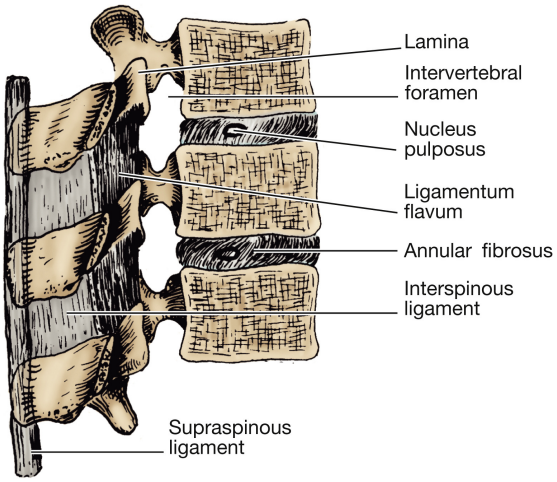

Figure 2.9: Illustration of the lumbar region bisected showing intervertebral and vertebral ligaments.

2.5 Ligaments

The spinal ligaments contribute to the vertebral column stability [21]. The ligaments' strength differs from region to region. The performance of a ligament is determined by its intrinsic morphology and the length of the moment arm through which it acts. The moment arm is the perpendicular distance between the line of action of the force and the centre of moments, given by

$$M = F.m \tag{2.1}$$

where M is the moment in Nm (Newton meter), F the force in N (Newton) and m the moment arm in m (meter). Thus, a weaker ligament with a longer moment arm may be just as strong as a stronger one with a shorter moment arm [20].

1. **Anterior longitudinal ligament**: broad strong ligament situated on the anterior surface of the vertebral bodies and intervertebral discs (figure 2.10, retrieved from [14]). It has the extension of all the spine length. This ligament is prone to injury in the cervical region, and has the function of preventing hyperextension of the spine and anterior herniation of the nucleus pulposus [20, 21].

2. **Posterior longitudinal ligament**: lies within the vertebral canal, on the posterior surface of the vertebral bodies and intervertebral discs (figure 2.10), having the length of the spine. This ligament prevents hyperflexion of the vertebral column and posterior herniation of the nucleus pulposus. It generally has the shortest moment arm, however, it has a high resistance to stress [20, 21].

3. **ligament flavum**: complex strong ligament that connect the laminae of adjacent vertebrae (figure 2.9 and 2.10, retrieved from [10] and [14] respectively). They are highly elastic,

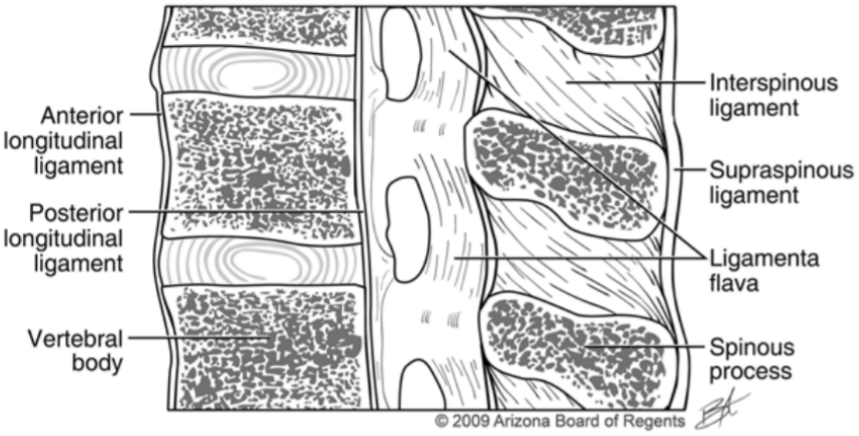

Figure 2.10: Major ligaments of the spine. Lateral view illustrating the ligament flavum, supraspinous, interspinous, and anterior and posterior longitudinal ligaments.

support the normal curvatures of the spine, and assist in extending the spine from a flexed position. However, due to its more ventral site of attachment and resultant shorter moment arm provide less flexion resistance. It facilitates the surgical exposure of the epidural space since it is deficient in the midline [20, 21].

4. **Intertransverse ligament**: connects the adjacent transverse processes [21], figure 2.9.

5. **Interspinous ligament**: connects the adjacent spinous processes [21], figure 2.9 and 2.10.

6. **Supraspinous ligament**: it is robust and binds the spinous processes together, figure 2.9 and 2.10. In the neck, the supraspinous ligament merges with the ligamentum nuchae [21].

7. **Capsular ligament**: encloses the facet articulating joints of the spine units, resisting to hyperextension and latetal bending [22].

On an emphasis note, the intertransverse, interspinous, and supraspinous ligaments help prevent hyperflexion and extreme lateral flexion of the vertebral column.

2.6 Muscles

The spinal musculature moves the torso by directly or indirectly affecting the spine, enabling complex vertebral movements. It also has the function of helping to maintain the posture to distribute the uneven force of the body's weight. They can be divided into extrinsic and intrinsic back muscle groups [9, 20].

In figure 2.11, retrieved from [14], a representation of the back muscles is presented. (A) On the left, the superficial splenius muscles; on the right, the erector spinae muscles, including iliocostalis, longissimus, and spinalis. (B) On the left, the transversospinalis muscles, including

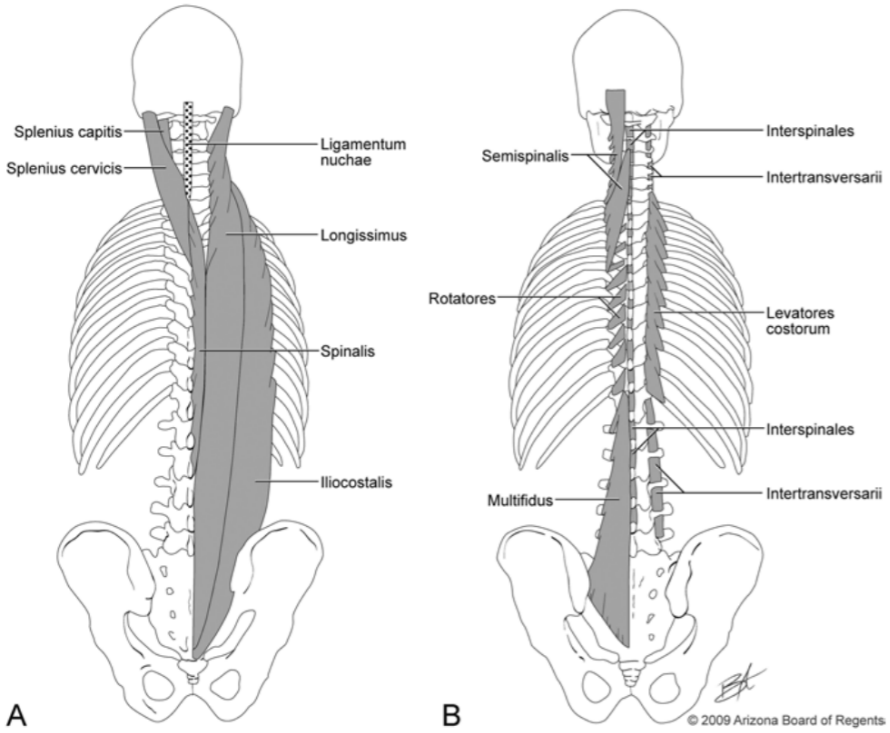

Figure 2.11: Back spinal musculature.

semispinalis, multifidus, and rotatores; on the right, the levatores costarum, intertransversarii, and interspinales muscles.

The extrinsic muscles are divided into superficial (trapezius, latissimus dorsi, levator scapulae, and the major and minor rhomboids) and intermediate (serratus posterior superior and serratus posterior inferior). The superficial are responsible for the movement of the upper limbs including movements of the scapula and humerus. Whereas the intermediate aid respiration since they are involved in the rib movement [9, 20].

The intrinsic back muscles are divided into superficial, intermediate, and deep. As main functions, these muscles maintain the posture and aid in the movement of the spine. The superficial layer is made of the splenius capitis and splenius cervicis. These are involved in neck flexion, rotation, and extension. The intermediate consist of the paraspinal or erector spinae muscles, the iliocostalis, longissimus, and spinalis. The erector spinae assist in extending and maintaining the central curvature of the spine. The deep layer includes muscles between the transverse and spinous processes of the vertebrae. The semispinalis is the most superficial and it is prominent in the thoracic and cervical regions. The multifidus is in the middle and it is the most prominent in the lumbar region. Lastly, the rotatores muscles are the deepest and the most prominent in the thoracic region [9, 20].

Lastly, it remains the suboccipital muscles (the rectus capitis posterior major, obliquus capitis superior, and obliquus capitis inferior). These are located deep in the back of the neck. They attach

Figure 2.12: Vertebral synovial joint.

to the skull and are involved in the movement of the head [20].

2.7 Intervertebral Joint

Looking at a motion vertebral segment (figure 2.4) it is understandable the relation between the two adjacent vertebrae. The articulations include the intervertebral disc anteriorly (between the bodies) and a pair of the facet or joints posteriorly, reinforced by ligaments.

The intervertebral disc articulation is a cartilaginous joint, which contains fibrocartilage (cartilage reinforced by additional collagen fibres), figure 2.8. It allows flexion, extension, and lateral bending motions, with slight movement [13, 19].

The articular facets joints are synovial, which contain fluid in a cavity surrounding the ends of articulating bones. The previous are classified as plane joints, or gliding joints, consist of two opposed flat surfaces that glide over each other, shown in figure 2.12 [13]. They provide slight uniaxial movement, being possible a very small rotation as well [13].

2.8 Nerves

The spinal cord (belongs to the central nervous system) is contained within the vertebral column. Thirty-one pairs of spinal nerves exit the spinal cord and pass through the intervertebral foramen to innervate the periphery, while meningeal branches of spinal nerves innervate the vertebrae. The spinal cord extends from the base of the brain to the end base of the spine, i.e., until the conus medullaris and filum terminale. The first is the cone-shaped end of the spinal cord and usually ends at L1-L2 in adults. In newborns, it ends at L3-L4. It is very important to know the ending location for surgical procedures, such as the lumbar puncture to reduce the risk of cord trauma. The second, filum terminale, is a delicate extension of the spinal cord from the conus medullaris that anchors to the dorsum of the coccyx [9].

Chapter 3

Spinal Behaviour

3.1 Spine Biomechanics

This section reflects what was reviewed at this point, from section 2.2 to section 2.8. It focuses on the biomechanics characteristics of the spine as a unit but considering all its elements which have their mechanic properties.

Firstly, biomechanics is the application of mechanics' principles to biology systems [23]. There are two main applications of biomechanics, human movement improvement and the prevention or treatment of the injury. Therefore, biomechanics can be also applied to movement safety, and its research is important to the medicine quest to prevent and treat injuries [24].

As mentioned before, the spine is the main load-bearing structure of the human musculoskeletal system. It has three fundamental biomechanical functions, the first is to guarantee the load transfer along the spinal column without instability, the second is to allow sufficient physiologic mobility and flexibility, and finally, to protect the spinal cord from damaging motions [25]. Consequently, it is important to understand how it works and what are its biomechanical limits in order to prevent serious and irreversible injuries or threat the existing ones, and avoiding possible worsening.

3.1.1 Mobility

Functional moveable units (subsection 2.2.3 in chapter 2) are present as a pair of cervical, thoracic and lumbar vertebrae, thus, allowing the spinal column's movement. Nonetheless, the sacrum and coccyx are each formed by the fusion of vertebrae, classified as immoveable [10]. The lumbar region of the spine has greater mobility than the thoracic spine. The mobility of the spine also depends on the state of the intervertebral discs (geometry, stiffness, fluid content, ageing and degeneration) and its viscoelastic properties. As seen in chapter 2, the state of ligaments and its viscoelastic properties, the articular facet joints and the posterior bony elements have an influence on the motion range [25].

The spinal movement can be divided into six components: three deflections and three rotations. Figure 3.1 (from [26]) is the exemplification of the physiologic motion segment planes and

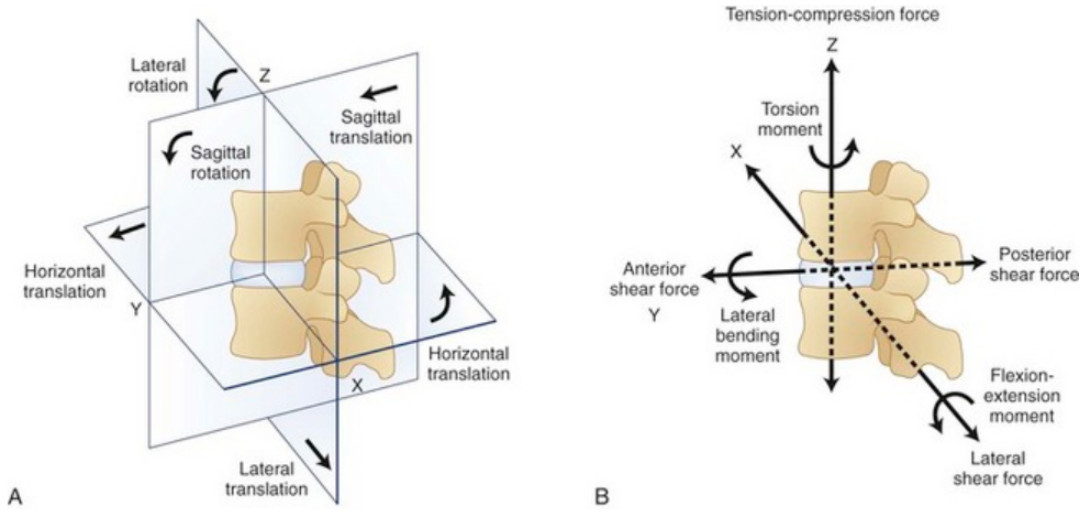

Figure 3.1: Spinal motion segment planes and directions of motion (A) and biomechanical coordinate system and direction of forces and moments (B).

respective motion directions, such as the lateral bending in the frontal plane, flexion and extension in the sagittal plane, and the rotation around the long axis of the spine. In addition, the spinal motions are characterized by the neutral zone, where the spine shows no resistance, the elastic zone, where the spinal resistance works, and the sum of both, the range of motion [25].

3.1.2 Stability

Spinal stability is important for characterizing and evaluating the spinal column and is critical for it to function properly. It is clinically defined as "the ability of the spine under physiological loads to limit patterns of displacement so as not to damage or irritate the spinal cord or nerve roots and, in addition, to prevent incapacitating deformity or pain caused by structural changes" [27]. Both static and dynamic stability must be considered. The first is defined in a system in static equilibrium (the sum all the vector forces is equal to zero). In the second, the system is moving along some trajectory, changing with time (the sum of the vector forces is equal the acceleration quantity Q). Stability can be evaluated by the presence or absence of a new behaviour secondary to small disturbances of force acting on the system. On a final note, stability is maintained by the musculoskeletal system (active), the spinal column (passive); and the neural system (which triggers the active system). Under normal conditions, the three subsystems maintain mechanical stability while the spinal column translates and rotates about the three cardinal anatomical axes (figure 3.1), enabling six degrees of motion [28].

3.1.3 Loads

There are two types of loads acting on the spine, they can be either physiologic or traumatic loads. The physiologic load, in turn, are present in the normal activity of the spine. They are classified as short-term loads (in flexion, extension), long-term loads (in sitting, standing), cyclic loads (in gait, walk), and lastly, dynamic loads (in running, jumping). On the other hand, when a sudden big impact with a great amplitude occurs, the resulting load is called traumatic. During a fall or other effects with acceleration or deceleration, the ordinary gravity load can be multiplied and, thus, cause a compression fracture, for example. Traumatic overload of the spine may cause irreversible damage in the discs and facet joints [25].

The back muscles prevent the spine from extreme injurious movements and loads(section 2.6) if the neural system has time enough to activate the muscles. For instance, due to abdominal muscle activity, the intra-abdominal pressure decreases the vertebral column compression. At the same time, the muscle contraction causes high compressive forces to the lumbar spine. A practical example is lifting and holding weights, which subjects the lumbar spine to high compressive load (depending on the horizontal distance of the load from the lumbar area). Adding up, long-term vibration and cyclical effects may also increase its compression, leading to structural changes and fatigue effects in the tissue of discs and vertebrae [25].

3.1.4 Mechanical Behaviour

Stress (equation 3.1) is the restoring force (F) of an object per cross-sectional area (A), in Nm^{-2} (Pa). It is directly proportional to the strain, which is the length of stretch divided by the original length (equation 3.2). Their relation is given in isotropic conditions by the Hooke's law (equation 3.3), which says that the stress is equal to the multiplication of the stress by the material's Young Modulus (E), in Pa. Thus, Young Modulus is related to the elasticity of a material undergoing tension or compression in only one direction [29].

$$\sigma = \frac{F}{A} \tag{3.1}$$

$$\varepsilon = \frac{\delta}{l} \tag{3.2}$$

$$\sigma = E.\varepsilon \tag{3.3}$$

The body movement in everyday simple or heavy tasks implies different types of strain:

1. **compression**: is the stress most present in the vertebral column, it happens when a structure is squashed [30, 31];

2. **tension**: it is not as common and it is defined as the force when stretch longitudinally [30, 31];

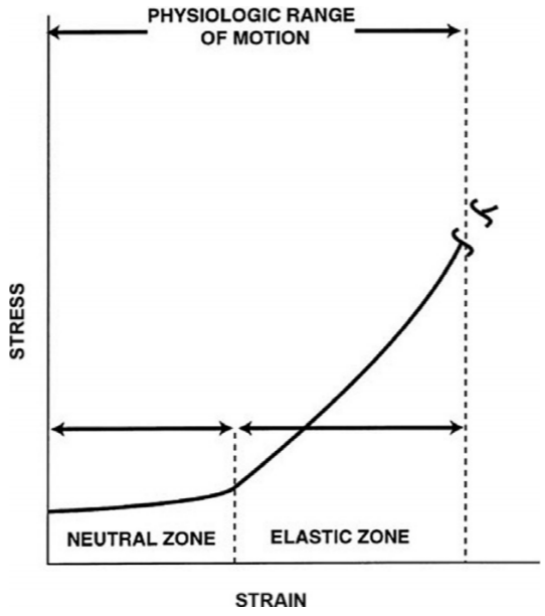

Figure 3.2: A typical stress-strain curve portraying the neutral and elastic zones.

3. **shear**, it can happen in the intervertebral discs when two vertebrae are forced to slide with respect to one another [30, 31];

4. **torsion** is a twist motion, it is caused by a torque. It is felt mostly on the disc's fibers, some are stretched, other get curved [30, 31];

5. **bending**, flexion/extension, results of a momentum applied on the disc [31].

These can lead to serious spinal injuries depending on the load applied and mechanical properties of the affected elements. The relation between the strain and stress is given by figure 3.2, when the maximum strain capacity of the neutral zone is reached, the tissues are then deformed according to Hooke's law (equation 3.3, until the plasticity phase, from that point on, any deformation is permanent, and further the material breaks. Another dimensionless mechanical property to have in consideration is the Poisson's ratio (equation 3.4), which gives the ratio of the transverse strain to the longitudinal strain [29].

$$\upsilon = \frac{\sigma_y}{\sigma_x} = \frac{\sigma_z}{\sigma_x} \tag{3.4}$$

3.2 Spinal disorders

There are different spinal clinical conditions, having different origins and range of pain and can compromise the mobility of the patient. Firstly, section 3.1.2 shows the importance of analysing the patient's stability in order to have proper spine diagnostic. When is the absence of stability, it can be referred to as instability, either chronic or acute.

Chronic instability can be subdivided. The first is the dysfunctional segment motion, which is characterized by dysfunctional motion that leads to a pain syndrome, however, it shows no progression of deformity; whereas the second, glacial instability, whose deformity progresses slowly.

Acute instability is caused by trauma and can be limited or overt acute instability. Limited instability allows the patient to continue the normal activities, and is defined as the loss of the integrity of either ventral or dorsal spinal portion, as happens in isolated laminar fractures or ligamentous disruption with intact ventral elements. As opposite, the overt instability is the inability of the spine to support the torso during normal activity. There is a loss of vertebral body or disc integrity combined with a loss of integrity of the dorsal elements. This type of instability requires surgical stabilization [28].

Spinal disorders, as follows, are classified accordingly to their cause. For instance, they can arise due to trauma, pathology, or normal aging [32]. Fractures are an example that the same condition was originated differently, it could be from a severe fall (traumatic) or from the aggravation of osteoporosis.

Osteoporosis: Demineralization of the bones. Severe osteoporosis increases the risk of developing a vertebral compression fracture [9].

Osteoarthritis: Most common of arthritis, which leads to the progressive erosion of joint cartilage. Can cause hyperextension of the cervical spine and compression of spinal nerves, followed by pain [9].

Spinal disc herniation: Discs may tear at the periphery along the annulus fibrosus leading to herniation of the internal nucleus pulposus. The symptoms are pain, numbness, weakness, and decreased reflexes [9].

Spinal stenosis: Narrowing of the central spinal canal. Can be caused by osteoarthritis, rheumatoid arthritis, Tuberculous spondylitis, or trauma. The are numbness, weakness, or pain in the upper or lower extremities [9].

Spondylolisthesis: Complete dislocation with anterior displacement of one vertebra on another [9].

Tuberculous spondylitis: Caused by tuberculosis. This is osteomyelitis of the vertebral bodies along with intervertebral discitis. Symptoms may include weakness of the lower limbs, kyphosis, back pain, fever, and weight loss [9].

Kyphosis: Increased anterior curvature (flexion) of the thoracic spine. Can have origin in osteoporosis, or tuberculous spondylitis and poor posture and often seen in the elderly.

Lordosis: Increased lumbar posterior curvature (extension). Caused by anterior trunk muscle weakness which is more common in late pregnancy and obesity [9].

Scoliosis: Abnormal lateral deviation and curvature of the spine. Happens when there is the absence of part of a vertebra or vertebral muscle weakness and may include abnormal rotation of one vertebra [9].

3.2.1 Thoracolumbar Fractures

Around 90% of spinal injuries involve the thoracolumbar region, also kwoun as dorso-lumbar region, which 50% occur between T11 and L1 [33], with an higher incidence on L1 [34]. Despite having many elements on the vertebral column that can suffer from a specific cause, vertebrae fractures are very common and are the cause of 15% of all trauma hospitalizations [35].

There are many classification systems for the thoracolumbar fractures, such as the McAfee, created in 1983 [36, 37], Magerl in 1994 [38], and the AO classification [39] (derived from the previous) in 2013. The last, AO classification incorporates both fracture morphology and clinical factors relevant for clinical decision making, and it will be used for the thoracolumbar fractures classification purpose.

These type of injuries are categorized into three groups: type **A**, compression injuries; **B**, distraction injuries;and **C**, displacement or dislocation. A and B are then subdivided according to the vertebra type of damage (see figure 3.3):

Type A fractures

A0 - Minor, nonstructural fractures — no or clinically insignificant fractures of the spinous or transverse processes, do not compromise the structural integrity of the spinal column;

A1 - Wedge-compression — they involve a single anterior or middle endplate without involving of the posterior wall of the vertebral body;

A2 - Split — also known as split or pincer type injuries; they involve both endplates without the involvement of the posterior wall;

A3 - Incomplete burst — they involve a single endplate along with the posterior vertebral wall; a vertebral laminar fracture is usually also present and does not constitute a tension band failure;

A4 - Complete burst — they involve both endplates along with the posterior vertebral wall; a vertebral laminar fracture is usually also present and does not constitute a tension band failure.

Type B fractures

B1 - Transosseous tension band disruption Chance fracture — they involve disruption of the posterior tension band with extension into the vertebral body;

B2 - Posterior tension band disruption — Bony and/or ligament failure of the posterior tension band together with a Type A fracture;

B3 - Hyperextension — they involve injuries to the anterior tension band and intervertebral or interosseous injury.

3.2.2 Complete Burst Compression Fractures

In this dissertation, the traumatic complete burst compression fracture (A4) of L1 vertebra will be considered. For that reason, from now on this review will be more focused on this type of fracture on L1.

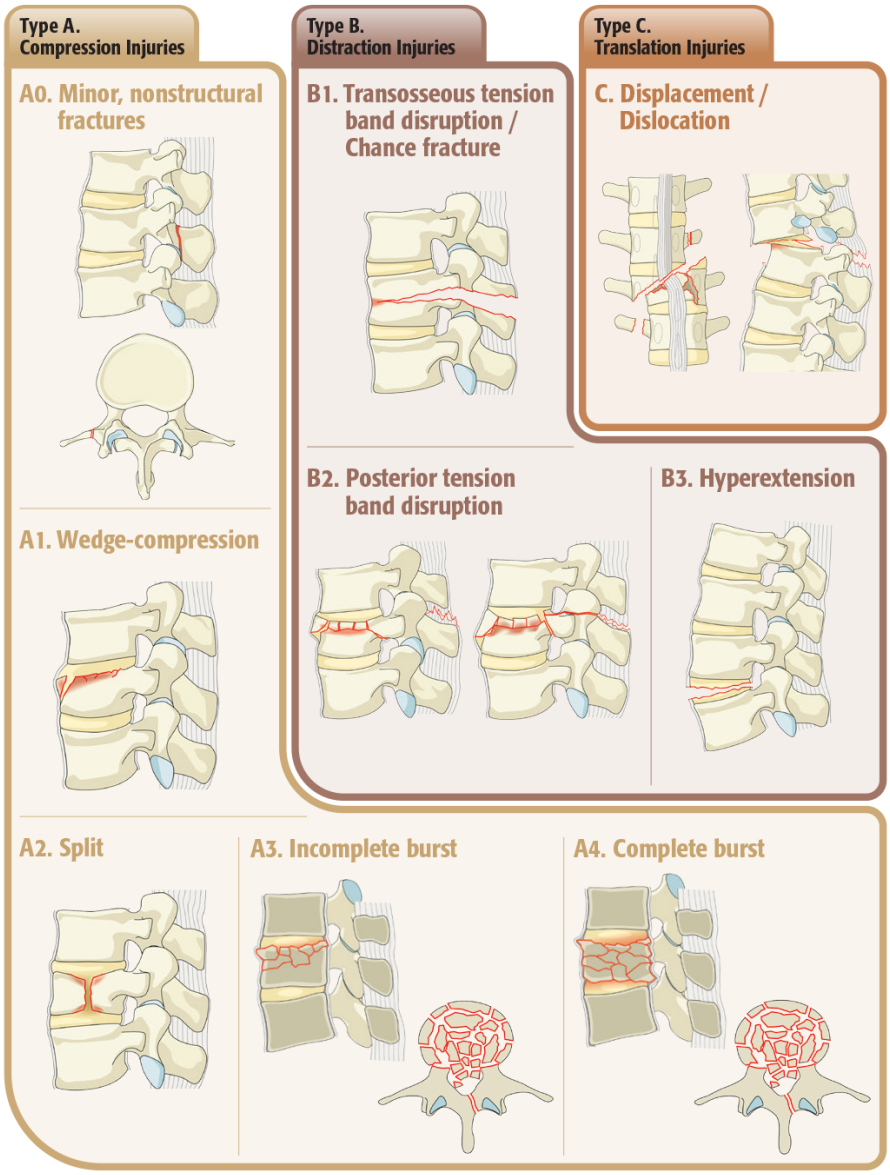

Figure 3.3: AOSpine Thoracolumbar Classification System (AO Foundation, Radiopaedia.org, rID: 59354, adapted).

Burst fractures occur during impact rather than during static loading and are more common in the upper and middle cervical and lumbar spine, in this case, the L1 vertebra this type of injury results from an axial loading force with no bending moment, presented in figure 3.4 [28]. In this case, the posterior elements are preserved, therefore, these fractures are not overtly unstable [28, 40]. However, each fracture is different, its instability classification relies on mechanical, neurological or both degrees [37, 41].

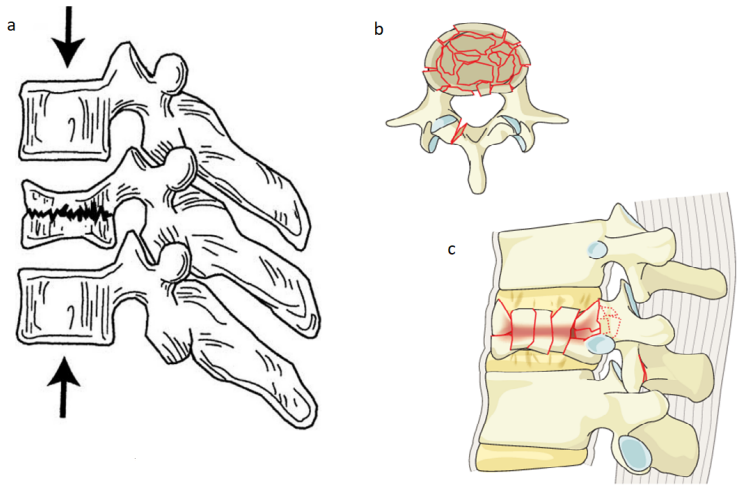

Figure 3.4: The mechanism of injury of a burst fracture: true axial loading without a bending moment (a). Superior (b) and lateral (c) views of a complete burst fracture.

3.3 Surgical Treatment

Most dorso-lumbar burst fractures are stable injuries that do not need surgical treatment. However, they can be considered unstable fractures associated with some degree of canal compression, leading to neurologic deficits manifestation. Many authors agree that this neurologic impairment is an indication for surgical decompression and stabilization of this type of unstable injury [42, 43].

It was proposed to study two surgical treatment approaches for the type A4 fracture on L1, the *Posterior Short Segment Fixation with Intermediate Screws* and *Posterior Long Segment Fixation*. Both treatments surgical steps and some considerations are tackled below.

3.3.1 Posterior Short Segment Fixation with Intermediate Screws

Posterior short segment fixation with intermediate screws is similar to the conventional posterior short segment fixation with the variation of the extra steps of the intermediate screws, as the name suggests. Some studies compare both procedures, Ji-wei Tian *et al.* concluded that the first restore fractured vertebral height with more efficiency, allows earlier ambulation, and it is also associated with a decrease in the segmental kyphotic angle [44]. The intermediate screws provide more biomechanical stability to the construct [45].

Any type of surgery needs preparation, in this case, before the treatment *per se*, the patient is anaesthetised, then placed prone with the abdomen suspended, and closed reduction is performed. Finally, to expose the lamina and facet joints a posterior midline incision is made over the aimed vertebra [44].

The following surgical treatments' steps are posterior to the preparation and are relying on the *AO Foundation Surgery Reference* [45], they are related to the reduction with pedicle screws, and all repeated on the opposite side.

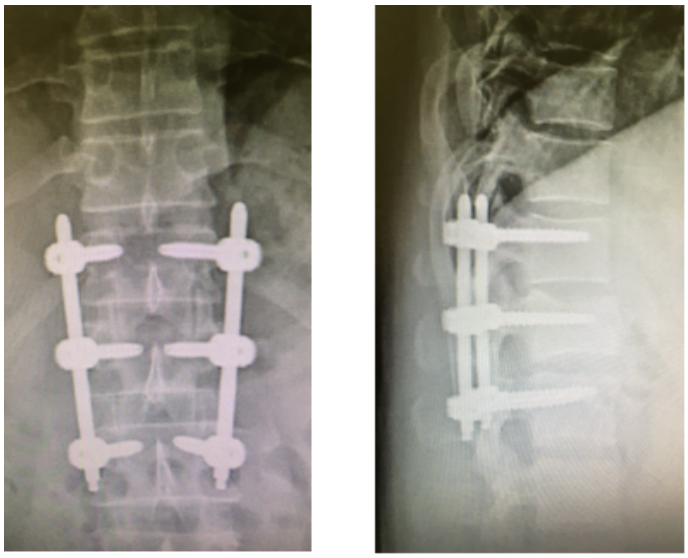

Figure 3.5: CT images of Posterior Short Segment Fixation with Intermediate Screws treatment in a posterior view (a) and a sagittal peripheral view (b).

1. **Pedicle screw insertion**

   Mono- or polyaxial screws are inserted into the vertebrae cephalad and caudal pedicles to the fracture level on both sides. The insertion of the screws technique is detailed explained in this chapter at subsection 3.3.3.

2. **Intermediate screw insertion**

   This can be seen as the "extra step" to other techniques. The intermediate screws are inserted into the healthy pedicles of the fractured vertebra. This technique cannot be used if both the pedicles are injured.

3. **Rod contouring**

   The contouring of the rod depends on the site of the fracture. In this case, a slightly lordotic or straight rod is chosen for fractures on L1.

4. **Rod insertion**

   The rod is introduced and tightened first to the most distal screw heads. Then it is inserted to the intermediate a proximal screw heads, by that order and are kept loose.

5. **Decompression**

   If decompression is needed, an indirect reduction may be done in this step. If it is insufficient, a transpedicular or posterior direct decompression is undertaken.

6. **Distraction**

   In this stage, the proximal screws are distracted along the rod. With the help of a distractor and a rod holder, on both sides simultaneously. In order to maintain that distraction, the locking heads of the proximal and intermediate screws are tightened.

Being a nonfusion surgery, during the entire procedure the facet joint capsule is preserved and no further steps are taken.

Two images of the *Posterior Short Segment Fixation with Intermediate Screws* treatment in both posterior and sagittal peripheral views are presented in figure 3.5. The broken vertebra is the L1, the middle vertebra with screws, the two adjacent screwed vertebra are healthy. Before wound closure, intraoperative imaging is performed to decide if the length of screws, the overall coronal and sagittal spinal alignment, reduction, and position are adequate.

Reported by Shaoyu Liu *et al.*, at the postoperative stage, most patients show functional neurological improvement and pain relief [42].

3.3.2 Posterior Long Segment Fixation

Mauro Dobrain *et al.* study on the inclusion of fracture level in a short-segment fixation, i.e., (*Posterior Short Segment Fixation with Intermediate Screws*) and long-segment instrumentation for thoracolumbar junction fractures concludes that both methods result in similar maintenance of the sagittal alignment and kyphosis correction [46].

Both presurgical preparations are equal since they refer to the same type of fracture and are executed in the same posterior plane. They also have almost the same surgical steps, as an exception of the second step (intermediate screws) of the reduction of the previous method, which is nonexisting in this one, and the screws and vertebrae quantity [47]. In this case, there are no screws in the injured vertebra, but they exist in the two above and two below.

1. **Pedicle screw insertion** In this technique, pedicle screws are inserted two levels above and below the fractured level on both sides.

2. **Rod contouring**

3. **Rod insertion** Here the rod can be inserted either from distal to proximal or vice versa. And the four distal screw heads are tightened.

4. **Decompression**

5. **Distraction**

Figure 3.6 shows two images of the *Posterior Short Segment Fixation with Intermediate Screws* treatment in both posterior and sagittal peripheral views. The broken vertebra is the L1, the middle vertebra between the screwed vertebrae. The two upper adjacent vertebrae and the two adjacent bellows are healthy.

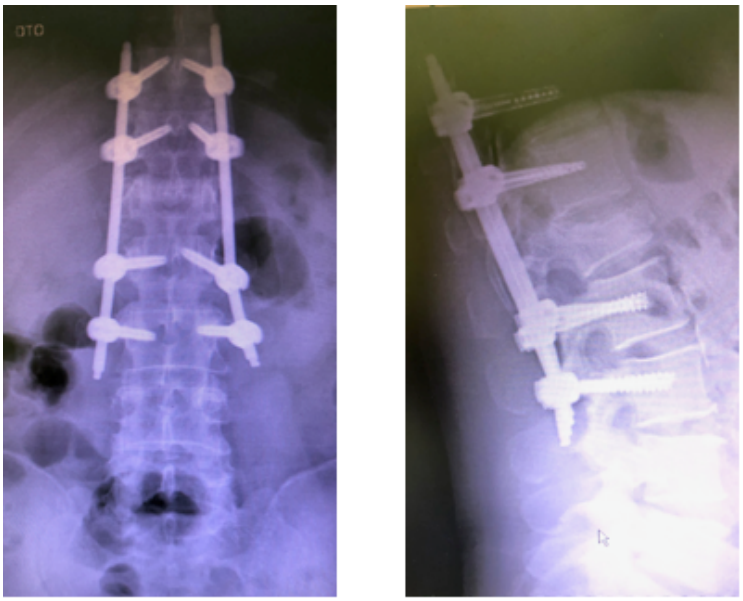

a b

Figure 3.6: CT images of Posterior Long Segment Fixation in a posterior view (a) and a sagittal peripheral view (b).

3.3.3 Screw Insertion Technique

In both techniques there is the requirement of understanding the vertebrae anatomy (chapter 2 section 2.3) due to the screw insertion through the vertebrae. In this section, the technique is explained accordingly to the *AO Foundation Surgery Reference* [48] from the drill location on the lumbar and thoracic vertebrae, to the adequate angles.

For the lumbar vertebra, the entry point of the pedicle screws is defined as the confluence of any of the four lines: pars interarticularis, mamillary process, lateral border of the superior articular facet and mid transverse process, as exemplified in figure 3.7a.

The entry point of the thoracic vertebra is presented in figure 3.7b. These depend on the determination of the mid-portion of the facet joint insertion and the inferior edge of the transverse process. The entry point is lateral and caudal to their intersection.

Once the superficial cortex's entry points are found, they are open using a burr. A pedicle probe is then used to navigate into the vertebral body until the pedicle isthmus. This probe follows the cranial-caudal direction by aiming for the contralateral transverse process. like is shown in figure 3.7c.

The mediolateral inclination depends on the vertebra rotation. The medial penetration of the spinal canal superficially and lateral or anterior penetration of the vertebral body cortex at the depth of insertion must be avoided. Additionally, it should be aimed for the two screws stay entirely in the cortex of the pedicles and vertebra body, and converge at the same time, as seen in figure 3.7d.

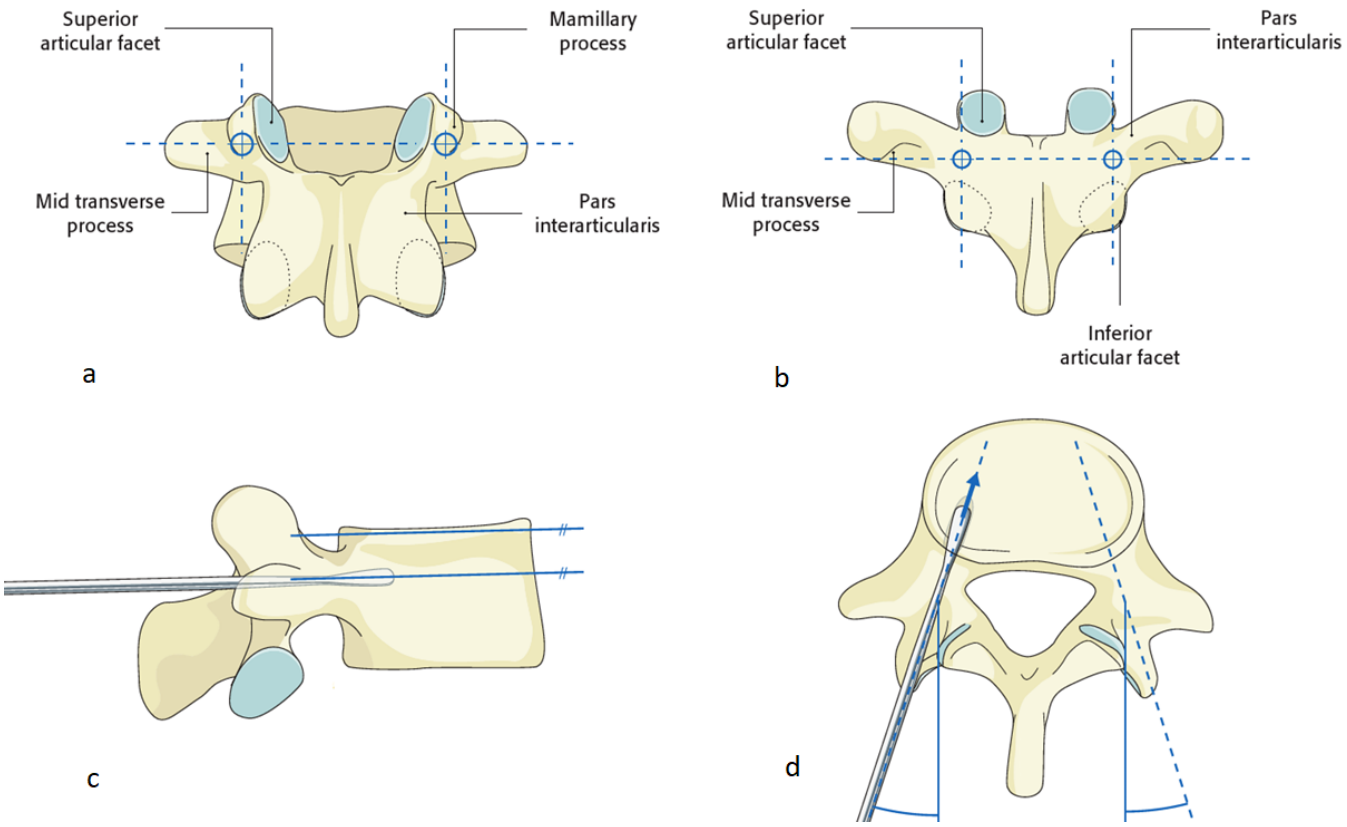

Figure 3.7: Illustration of lumbar(a) and lower thoracic(b) vertebrae entry points; cranial-caudal angulation(c); and medio-lateral inclination(d). *AO Foundation*.

Lastly, a mono or a polyaxial screw of appropriate diameter and length is carefully inserted into the same created trajectory.

3.3.4 Healing Classification

In this case study, the instrumentation is removed 18 months after the surgery if proven a total healed vertebra. This examination relies on the stability of the healed vertebra, if stable, it is considering a type I and II healing, whereas type III has healing potential and has yet to achieve type II, type IV is overly unstable and is in this case that the instrumentation is preserved [49].

Chapter 4

Three-Dimensional Finite Element Modelling

This chapter portrays the work done to achieve the present dissertation's purpose, the biomechanical comparison between two different L1 fixation methods, short with intermediate screws and long, explained in chapter 3.

Firstly, it is shown the healthy dorsolumbar column modelling and simulation, prior to any other, from the 3D shell construction of each component: T11, T12, L1, L2 and L3 vertebrae, intervertebral discs, endplates and ligaments; through the FE model; and at last, all the loads, contact and boundary conditions.

The same approach is given to the pathological model, short and long treatment models. Their major difference from the intact model relies on the L1 broken vertebra, which simulates the complete burst fracture (A4 type in the AO classification). For the last two, there are additional components: screws and rods, thus, their contact conditions. Both models have the initial and final post-surgery approach, where the contact conditions are described accordingly.

The intact model is the base for the pathological model, while the treatment models rely on the pathological. Since some steps are the same, throughout this chapter, the explanation will not be repeated nor the corresponding figures. However, when it is appropriate, that same aspect will be pointed out.

Resuming, each model will be described through its vertebrae, intervertebral discs and endplates, ligaments FEM modelling, respective mechanical properties, boundary and contact conditions, and the load applied.

4.1 Intact Dorsolumbar Model

The intact dorsolumbar model is a recreation of a healthy dorsolumbar spine, i.e., with no pathologies associated from T11 to L3. It was the first model modelled, before recreating any spinal condition as the others are reconstructions of this healthy one.

4.1.1 Components FEM Modelling

4.1.1.1 Vertebrae

The first aspect taken into account was to enable CT images of a healthy column, of a 30 years old man. These images were then processed in the *Mimics* software with the area of interest, i.e., from T11 to L3 vertebrae. The contrast was controlled, Gaussian filters were used, as well as morphological filters, resulting in vertebrae split, the final mask in a sagittal cross-section represented on figure 4.1 (left).

Mimics software files were exported containing the 3D shell of each vertebra and imported to the *Meshmixer* software for deleting intersections, reducing the volume and achieving smooth shells. Finally, the four-node tetrahedral elements (C3D4) mesh of each solid vertebra was created in the *Abaqus/CAE* software, as seen on the right side of figure 4.1.

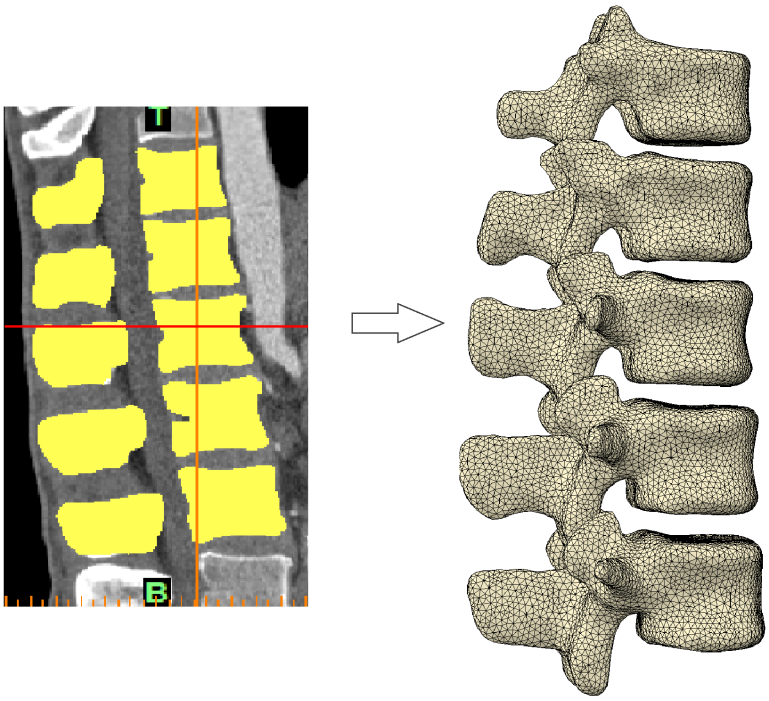

Figure 4.1: The 3D vertebrae achieving process, from *Mimics* (left) to *Abaqus/CAE* (right).

Further, using again the *Mimics* software, the elements were differentiated in trabecular, inner elements, or cortical bone, outer elements, according to the histogram values of the CT images. The upper and lower vertebral layers are called vertebral endplates, subchondral bone overlaying the trabecular bone [50].

As a representation of all the vertebrae, the L1 vertebra's coronal view is present in figure 4.2, where the darker inner elements are trabecular, and the lighter outer elements are cortical.

Table 4.1: Intact vertebrae's number of elements

Vertebrae	*Cortical*	*Trabecular*	*Total*	*Elements' Type*
T11	35592	24343	59935	
T12	36080	18080	54160	
L1	42881	19463	62344	C3D4
L2	49797	20536	70333	
L3	55066	19382	74448	

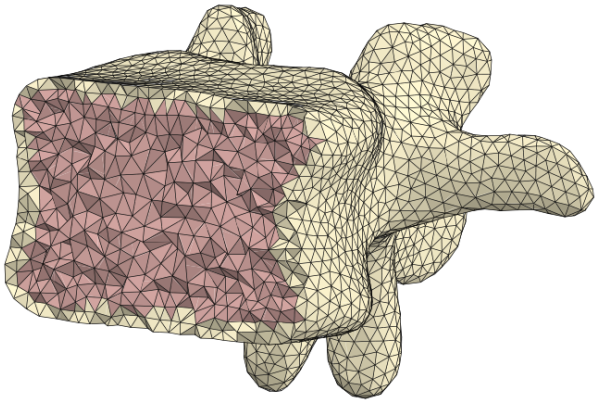

Figure 4.2: Coronal cut view of L1 vertebra.

The number of vertebral elements is explicit in table 4.1, where the total elements are the sum of the cortical with the trabecular. It shows that the lumbar vertebrae have more volume when compared with the thoracic vertebrae.

Despite the trabecular area in figure 4.2 implying a larger section than the cortical, the disproportional values in table 4.1 are explained by the cortical posterior elements of the vertebra.

4.1.1.2 Intervertebral Discs and Endplates

The intervertebral discs have low density, therefore, they were not visible in the CT images. Therefore, it was necessary to recreate them via modulation. From the *Meshmixer .stl* file, the vertebrae were all imported to the *Rhinoceros 6.0* software. Knowing that the intervertebral disc site is between two consecutive vertebrae, those were made primarily from two polylines following each vertebral endplate perimeter. From that, two vertical curves uniting the previous polylines were swept through those, creating the outer surface of the annulus fibrosus. Repeated in all spaces between the vertebrae, T11-T12, T12-L1, L1-L2, L2-L3, making a total of four intervertebral discs.

Similarly to Chen C *et al.* (2001) [51] who reported that the nucleus pulposus is 30% to 50% of the total disc area, the area delimited by the inner surface of the annulus fibrosus is 40% (outer surface of the nucleus). The area held by the two surfaces was divided equally eight times,

resembling the discs fibres. As reported by Marchand F and Ahmed AM (1990) [52], there are many crosslinked fibres, that would be almost impracticable to replicate. Nonetheless, the same authors detected up to eight peripheral layers, recreated in this work. These nine surfaces are illustrated in figure 4.3a. The intersection of the outer fibre surface with the vertebral endplates' surface created the final stage of the disc solid, the upper section of figure 4.3b.

Between the disc and the vertebral endplate resides the cartilaginous endplate, which covers the nucleus and the inner fibres of the disc. This happens in the superior and the inferior regions of the disc, with a thickness between 0.5 and 1 mm [50, 53]. Thus, in the *Rhinoceros 6.0* software, the exterior surface of each endplate was achieved by the intersection of the disc horizontal surface with the vertical 4th fibre surface, shown in the middle image of figure 4.3b. From an inner 0.5 to 1 mm offset of the recent outer surface, each inner horizontal endplate surface was created. At last, the vertical surface which closes the endplate was possible by trimming the lateral surface of the fibre with the outer and the inner surfaces of the endplates, this final shape of two endplates of the same disc is represented in the last set of images of figure 4.3b.

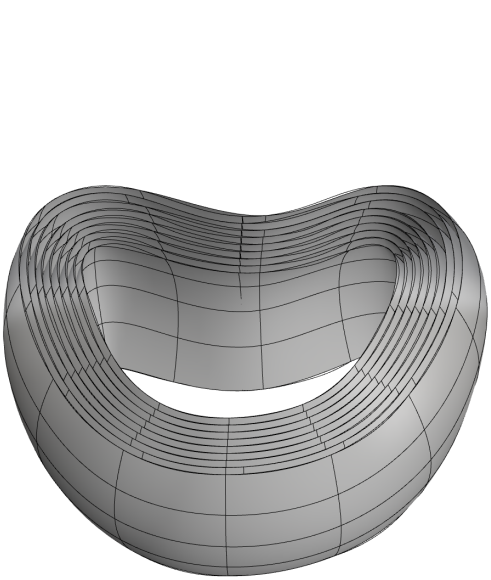

(a) Annulus fibrosus modulation.

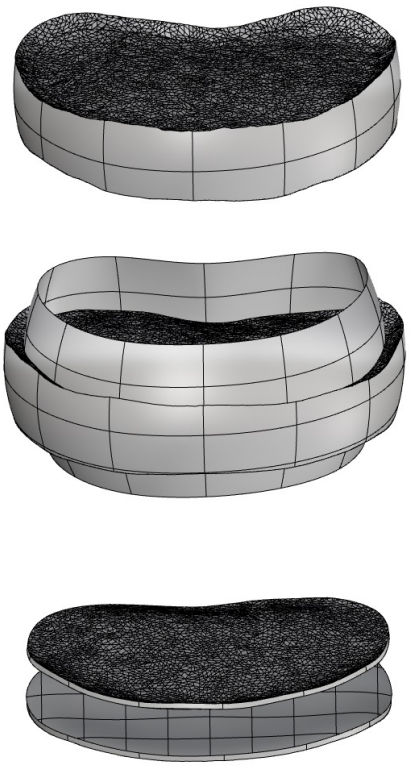

(b) Cartilaginous endplates modulated from the intersection of a intervertebral disc with a fibre surface.

Figure 4.3: Intervetebral disc and endplates modelling.

The solids (discs) and endplates *.stp* files, and the surfaces (fibres) *.igs* were then imported to *Abaqus/CAE* software as a part. Here the remaining area trespassing the disc cage was trimmed

up to the endplates/disc surface, forming, the eight fibres earlier presented, and the nucleus. Each part was meshed with hybrid, three-dimensional tetrahedral elements C3D4H, later classified in cartilage, nucleus pulposus and annulus fibrosus properties. The three structures can be clearly detected in figure 4.4, on the left, an exploded view allows the perception of the position of the nucleus relative to the fibres; on the upper right side, the outer view of the part; and, finally, the coronal cross-section of the part, being noticeable the thickness ratio between each component.

The same figure can be correlated with both table 4.2 and 4.3. The less complex bigger section is the nucleus, with larger elements and the smaller sections, the fibres and endplates, composed of smaller elements. Therefore, when comparing each section number of elements, despite the volume differences, the nucleus matches the same number as the endplates. On the other hand, the fibres have a greater volume and by adding the smaller elements, sum the biggest amount of elements as expected.

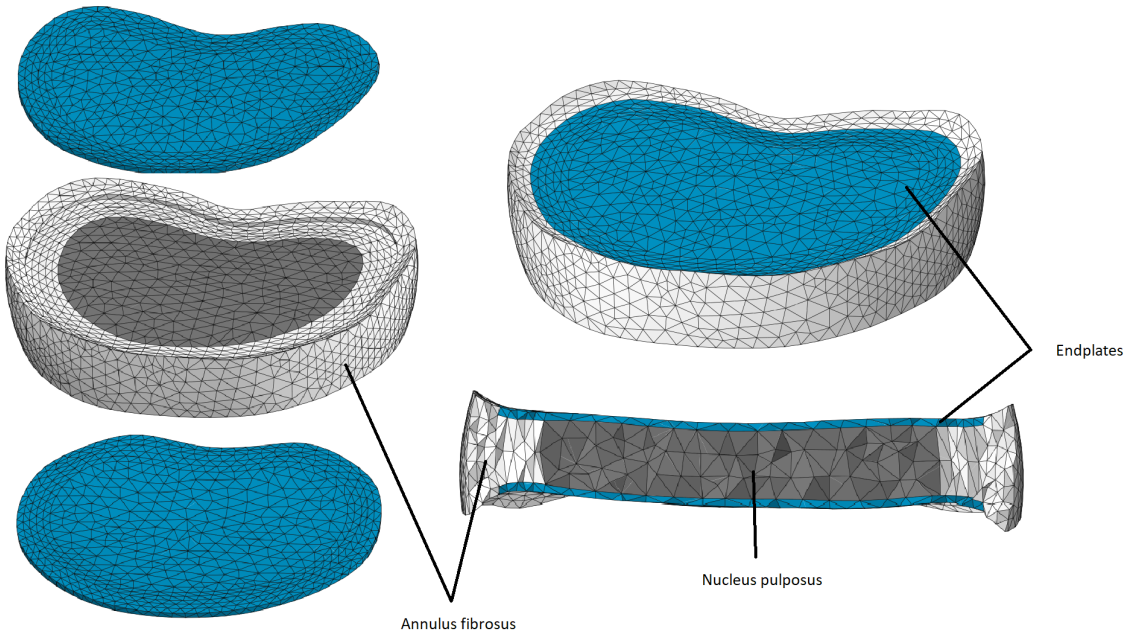

Figure 4.4: Endplates, nucleus pulposus and annulus fibrosus mesh.

Table 4.2: Intervertebral discs' number of elements

Region	*Nucleus Pulposus*	*Annulus Fibrosus*	*Elements' Type*
T11-T12	3622	10433	
T12-L1	4028	10587	C3D4H
L1-L2	5747	16279	
L2-L3	7948	16727	

Table 4.3: Intact cartilaginous endplates' number of elements

Region	*Superior*	*Inferior*	*Elements' Type*
T11-T12	3089	3163	C3D4H
T12-L1	3275	3217	
L1-L2	3928	3782	
L2-L3	3846	3465	

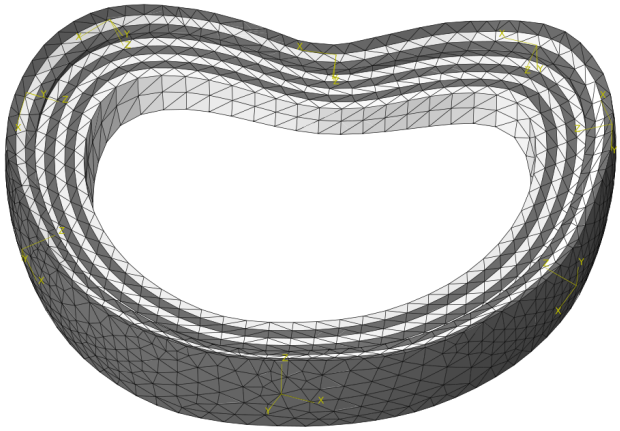

Figure 4.5: Fibres' different orientations and datums.

Marchand F and Ahmed AM (1990) [52] also discovered that the average fibre bundle angle corresponded to 30º to the horizontal plane. These collagen fibres reinforce the viscous annulus by creating a crisscrossing network. In order to mimic that aspect, each layer of the annulus fibrosus has an alternating orientation of ± 30º. Antecedent, the annulus was divided into eight concentric parts, each one had a correspondent datum. From the before-mentioned, the alternating ± 30º angles were created using such 3D coordinates systems, as shown in figure 4.5, the light fibres have a 30º orientation, and the darker a -30º orientation.

4.1.1.3 Ligaments

As presented in the chapter 2 section 2.5, many ligaments contribute to the vertebral column stability, especially the seven that were modelled: the anterior longitudinal ligament (ALL), capsular ligament (CL), interspinous ligament (ISL), intertransverse ligament (ITL), ligament flavum (LF), posterior longitudinal ligament (PLL) and supraspinous ligament (SSL).

These ligaments were first modelled in the *Rhinoceros 6.0* software as lines and are further meshed as a 2 node linear 3D truss element (T3D2) in the *Abaqus/CAE* software. Each ligament was divided according to [54], corresponding to the number of elements' column in table 4.4.

Each cross-sectional area, in mm^2, is the quotient of the total ligament area in [55] divided by the number of elements.

The cross-sectional area is discernible in figure 4.6a where the ALL are bigger than ITL, and in figure 4.6b SSL is thicker than CL and ISL. The remaining ligaments are not visible in both figures, the reason being their placement between the vertebral body and superior and inferior vertebral notch.

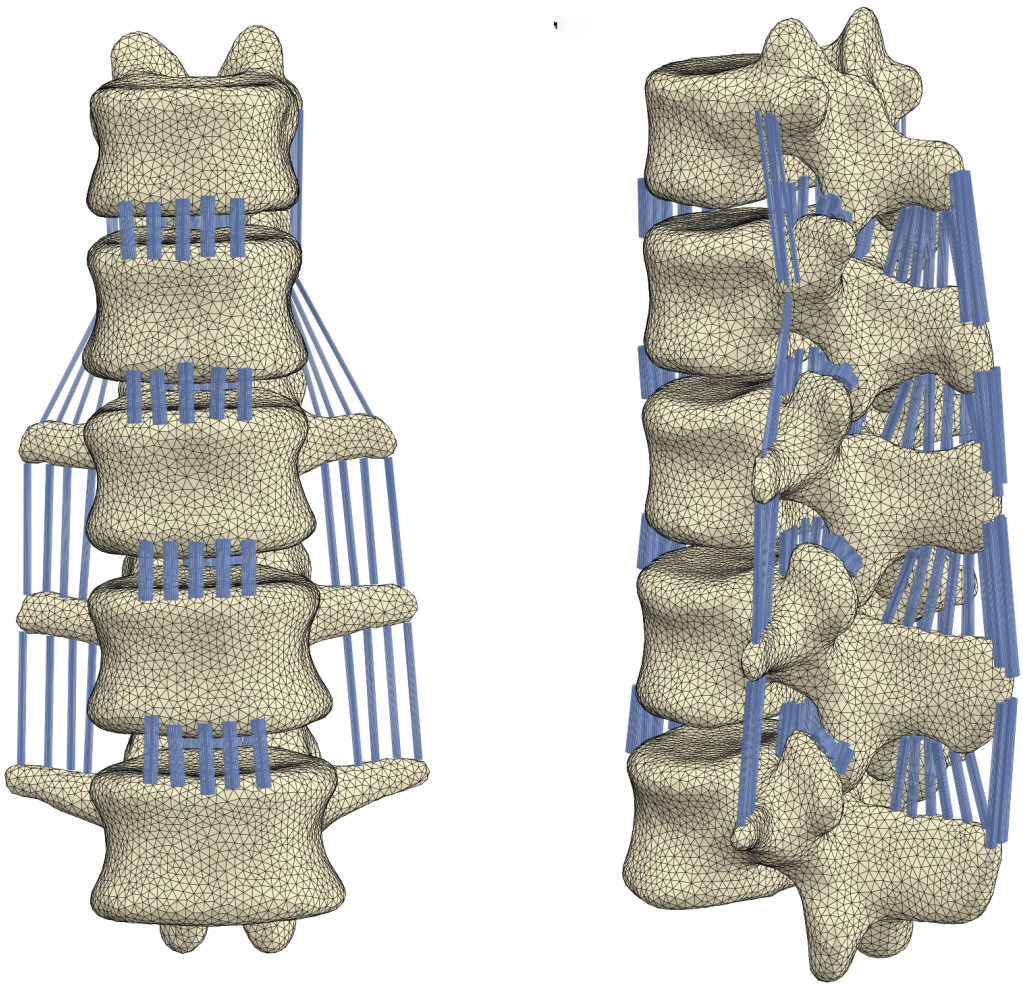

(a) Frontal view.

(b) Lateral view.

Figure 4.6: Vertebrae and respective ligaments.

Table 4.4: Ligaments' number of elements

Type of Ligament	Number of Elements*	Cross-sectional Area [mm^2]**	Total Number of elements
ALL	5	8.00	20
CL	6	5.00	48
ISL	6	6.67	24
ITL	4	2.50	16
LF	3	13.33	12
PLL	5	4.00	20
SSL	3	10.00	12

* Each large ligament was divided into a number of smaller ligaments [54] corresponding to the number of T3D2 elements.

** The section area of each small ligament, obtained from the number of ligaments and total area [55].

4.1.1.4 Intact FEM full model

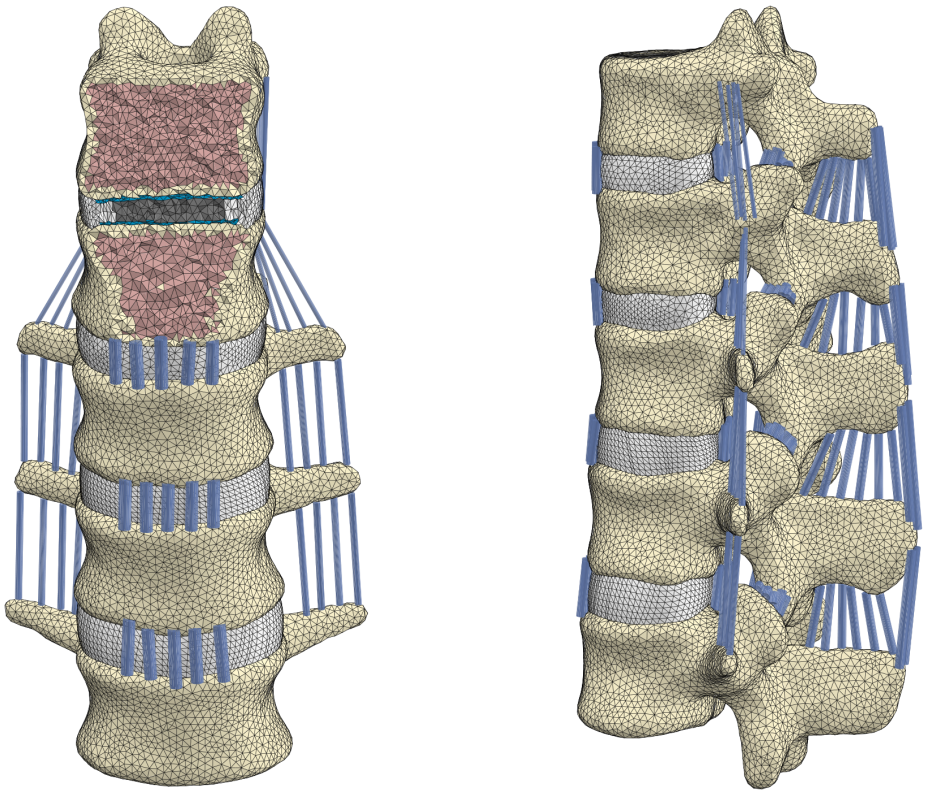

(a) Anterior view with a diagonal cut (b) Lateral view

Figure 4.7: Intact finite element model of the dorsolumbar spine.

To better understand all the steps described untill this point, the full representation of the final 3D FEM model is shown in figure 4.7. Here all the components of the column from T11 to L3 are

shown: vertebrae, intervertebral discs, endplates, ligaments, further described. Figure 4.7a is the anterior view of the model, with a diagonal cut on the T11 and T12 functional unit for visualization purposes. The lateral view is shown in figure 4.7b in order to observe the spinous processes and their ligaments, and the articular processes.

4.1.2 Mechanical Properties

After the modulation of each part emulating the real spine, every element was granted a mechanical property to behave like its corresponding real version. Some properties are given in a range of values because of the validation conclusions, shown in chapter 5 section 5.1, achieving the most reliable results.

On the one hand, the bone, the cartilage and the ligaments are elastic materials, mentioned in table 4.5 their Young Modulus and Poisson Ratio. The ligaments have no compression attributes, modifying only the elastic response of the material.

On the other hand, the intervertebral disc elements are hyperelastic materials, table 4.6. The nucleus pulposus behaves as an incompressible material. Hence, the isotropic Neo-Hookean model was the best fit, with material constants of C_{10} = 0.16 MPa and D = 0.024 $[MPa^{-1}]$ [54]. The fibre network, annulus fibrosus, has anisotropic materials, in consonance with the Holzapfel–Gasser–Ogden uniaxial properties: C_{10} = 0.035 MPa, k_1 = 0.296 MPa, k_2 = 65 MPa [56].

Table 4.5: Elastic mechanical properties

Elastic Component	Properties		Ref.
	Young Modulus (E) [MPa]	Poisson Ratio (υ)	
Cortical Bone	12000	0.3	[57]
Trabecular Bone	100	0.2	[57]
Cartilaginous endplates	24	0.4	[58]
ALL	20-75	0.3	[59, 60]
CL	7.7-20	0.3	[59, 60]
ISL	3.4-28	0.3	[59, 60]
ITL	10-50	0.3	[59, 61]
LF	2.4-10	0.3	[60, 61]
PLL	20-70	0.3	[59, 61]
SSL	3.4-28	0.3	[59, 60]

Table 4.6: Hyperelastic mechanical properties

Hyperelastic Component	C_{10} [MPa]	D $[MPa^{-1}]$	k_1 [MPa]	k_2 [MPa]	k	Ref.
Nucleus pulposus	0.16	0.024	-	-	-	[54]
Annulus fibrosus	0.035	0	0.296	65	0	[56]

4.1.3 Contact Conditions

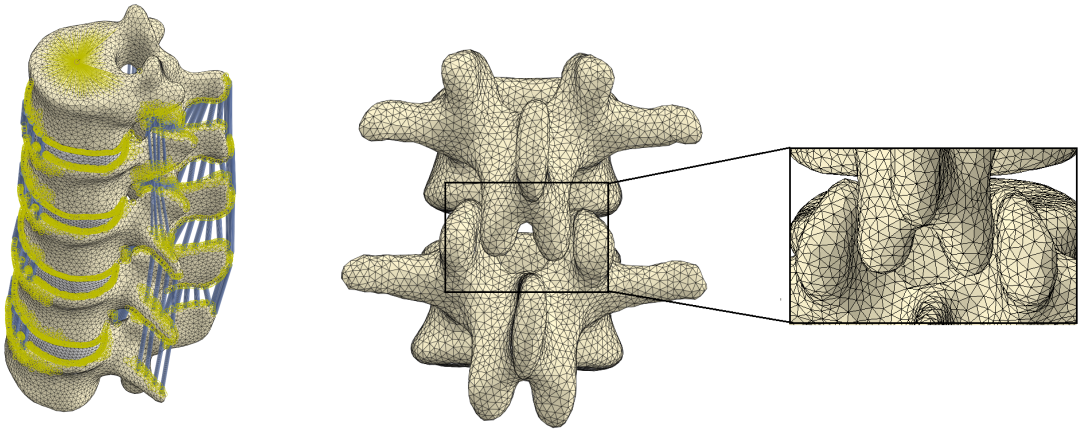

(a) All the intact model contacts.

(b) Facets' articulation.

Figure 4.8: Dorsulumbar FE model contact conditions.

All created parts were connected with multiple contacts with each other (figure 4.8a) in order to simulate the wanted intact spinal biomechanic unit.

Firstly, it was created the needed surfaces for every functional unit contacts from the vertebral endplates, cartilaginous endplates and annulus fibrosus. The interaction between the vertebral endplate and the disc + endplate was created with a *tie*. Since the disc + endplates have a more complex structure, their surfaces were the master and the vertebral endplate surface was the slave. This step was carried out for all the vertebral endplate-disc pair, i.e., T11 endplate with the superior surface of the first disc + endplate; the lower surface of the same disc with the superior endplate of T12; and so on up to the superior vertebral endplate of L3. That way, it was carried four intervertebral joints.

Secondly, each node of the ligaments was tied to the respective surface of their placing vertebra. The ALL nodes were tied to the anterior portion of each vertebral body, right above or under the intervertebral disc, and the PLL nodes were tied to the same posterior portion, resembling a disc cage. The LF nodes were tied with the anterior laminae parts of two adjacent vertebrae. The ISL nodes, as the ligament name suggests, ties above with an under spinous process surface, and under with an upper spinous surface. Once again, as the name suggests, the SSL nodes were tied with the posterior spinous process surfaces. The transverse processes' surfaces were tied similarly to the ITL nodes. At last, the CL nodes are crucial to the facets articulation enclosure, as they were tied to two adjacent facets.

Finally, to simulate the movement of the facets' articulation, i.e., the interaction between two adjacent vertebral facets, figure 4.8b, it was generated a general contact interaction on each pair of surfaces.

4.1.4 Boundary Conditions

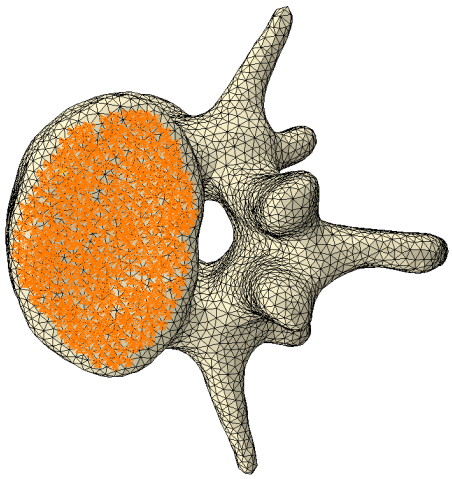

Figure 4.9: L3 inferior vertebral endplate fixation as a boundary condition.

Considering that the final purport of this T11-L1 model is to behave as a regular dorsolumbar column when a load is applied, it is necessary to employ the correct boundary conditions.

While the loads are applied on the T11 superior vertebral endplate, the bottom of the model must be completely fastened, to obtain reliable results. Therefore, as a displacement/rotation boundary condition on the initial step, the distal L3 endplate nodes were fixed in space, as shown in figure 4.9, according to a standard right-hand Cartesian coordinate system.

4.1.5 Load

As mentioned before, the load, which allows the vertebral movement, is applied in the superior T11 endplate, as exemplified in the figure 4.10, is represented as the reference point P. The aim to distribute that load from P through the endplate nodes is only accomplished with the *Coupling* function, yellow lines in figure 4.10.

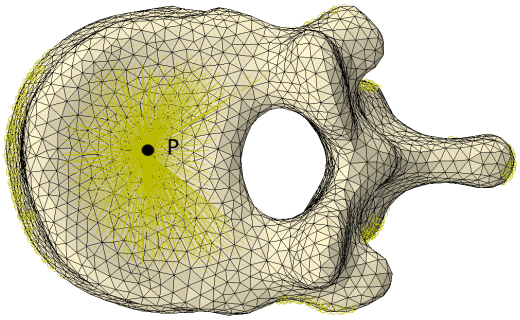

Figure 4.10: Coupling application on T11 superior endplate.

At long last, the loads applied in the reference node P referred to the Cartesian system of one plane coincident with the superior endplate. It was considered five momentums with the same intensity of 5 Nm but in different directions, the extension, the flexion, the lateral bending and the axial rotation.

4.2 Complete Burst fracture Model

In chapter 3, subsection 3.2.2 and subsection 3.2.1, refer to the complete burst fracture, A4 in the AO classification, as a compression fracture whose endplates are corrupted. Since there are two types of endplates, vertebral and cartilaginous, both supeior and inferior pairs of the L1 vertebra were excluded from the previous intact model. Also, a circumstantial volume of the lower third of the vertebral volume was withdrawn, so it would simulate an unstable vertebra.

Given the differences between the intact model and the pathological one, all the making processes, as well as the mechanical properties, contact, boundary and load conditions were maintained. Therefore, in this model's section, there will be a stronger focus on the vertebral and discal differences.

4.2.1 Components FEM Modelling

4.2.1.1 Vertebrae

All the vertebrae from the intact model are the same as this pathological model, except the L1 vertebra, which simulates a complete burst fracture. In this case, starting from the already modelled intact vertebra, its elements which constituted both vertebral endplates and the third bottom of the vertebral body were deleted, as shown in figure 4.11, this method is similar to the Wang *et al.* aprroach [62].

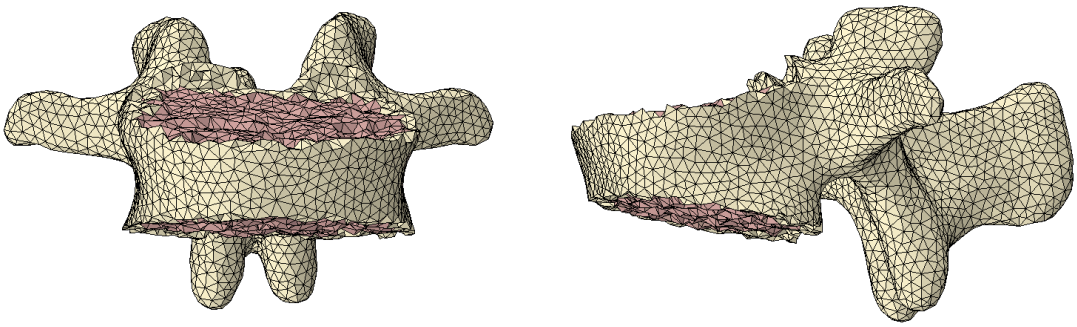

Figure 4.11: FE L1 with a complete burst fracture frontal (left) and lateral (right) views.

Comparing the L1 elements in table 4.7 with table 4.1, the cortical difference is higher than the trabecular, reason being the fact of the cortical endplates' property. The small difference in

trabecular elements derives from the minor body volume deletion, whose significant portion of elements had trabecular properties.

Table 4.7: Complete burst model's vertebrae's number of elements

Vertebrae	*Cortical*	*Trabecular*	*Total*	*Elements' Type*
T11	35592	24343	59935	
T12	36080	18080	54160	
L1	31805	11372	43177	C3D4
L2	49797	20536	70333	
L3	55066	19382	74448	

4.2.1.2 Intervertebral Discs and endplates

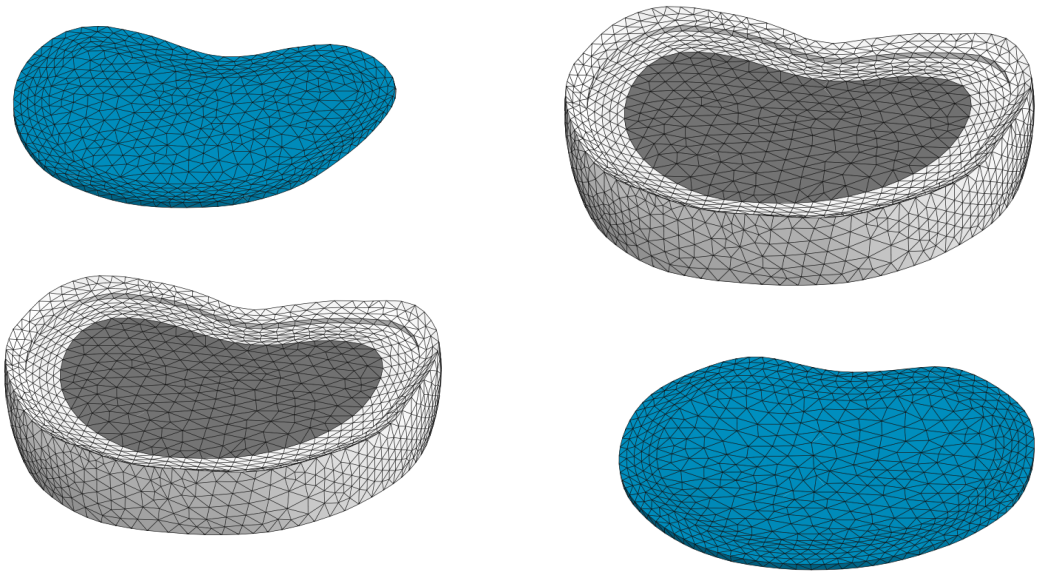

(a) T12-L1 disc

(b) L1-L2 disc

Figure 4.12: T12-L1 (a) and L1-L2 (b) regions intervetebral disc and endplates modelling.

The intervertebral discs of this model are equal to the intact model, whereas the endplates are not. The two adjacent cartilaginous endplates to the L1 vertebra were excluded from the pathological model. Hence, in the T12-L1 section, only the T12 adjacent endplate is present, as seen in figure 4.12a; while in the L1-L2 region, the only existing cartilaginous endplate is the one facing the L2 vertebra.

Table 4.8: Burst cartilaginous endplates' number of elements

Region	*Superior*	*Inferior*	*Elements' Type*
T11-T12	3089	3163	C3D4H
T12-L1	3275	**N/A**	
L1-L2	**N/A**	3782	
L2-L3	3846	3465	

In a summary manner, table 4.8 shows a not applicable (N/A) value in the non existing endplates. The remainder continued with the same number and type of elements.

4.2.1.3 Complete burst FEM full model

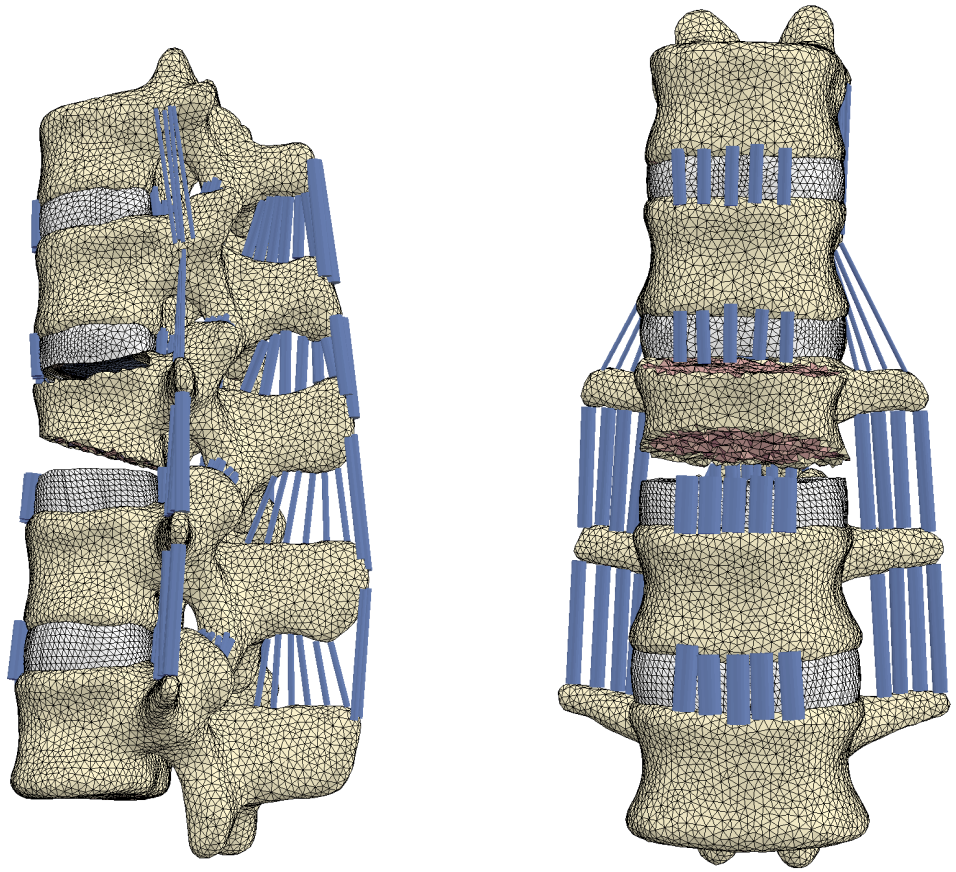

(a) Lateral view

(b) Anterior view

Figure 4.13: FE Complete Burst fracture Model.

Figure 4.13 shows the full complete burst FEM model after modelling, achieved through the methods explained so far. Both lateral and anterior view show the L1 complete burst fracture.

4.2.2 Mechanical Properties

All the parts' mechanical properties were retained from the intact model, except the *deleted* L1 vertebra elements and the ALL ligaments.

When referred to the deleted elements, this implies the simulation of void elements. The Poisson ratio reduction to nearly zero makes this elements section compressible. The Young Modulus is 8000 times less than the bones', making the elements more flexible, being easily stretched or bent.

Once too compressible, the elements only maintain these properties when a load is applied if there is no rigid body attached with a countered force. Hence, the ALL ligaments which overlapped the void ligaments (T11-L1 and L1-L2 ALL) were considered also flexible with Poisson ratio and Young Modulus close to zero.

4.3 Posterior Short Segment Fixation with Intermediate Screws Model

The Posterior Short Segment Fixation with Intermediate Screws (PSS) model has two modelling screws in the T12, L1 and L2 vertebrae. Thus, these three vertebrae are the only ones that differ from the pathological model.

For those reasons, it will be placed great emphasis on the fixed vertebrae, the screws and rods, which allow the fixation, moreover their mechanical properties and contact conditions.

4.3.1 Components FEM Modelling

4.3.1.1 Pedicle screws and rods

The screws must be structurally strong to be able to manage all the load scenarios. The screw must be fitted to its final vertebra. The diameter is chosen according to the pedicle width, which must be at least 0.5 mm smaller than the outer pedicle width to ensure safe transpedicular screw installation [63]. Also, it is crucial to know the distance from the outer pedicle to the anterior cortical area in order to know the pedicle screw length to use and prevent vascular or visceral complications [64, 65]. The dorsolumbar screws can go from 4.0 mm to 6.5 mm in diameter, and 30 mm to 45 mm in length [66, 67].

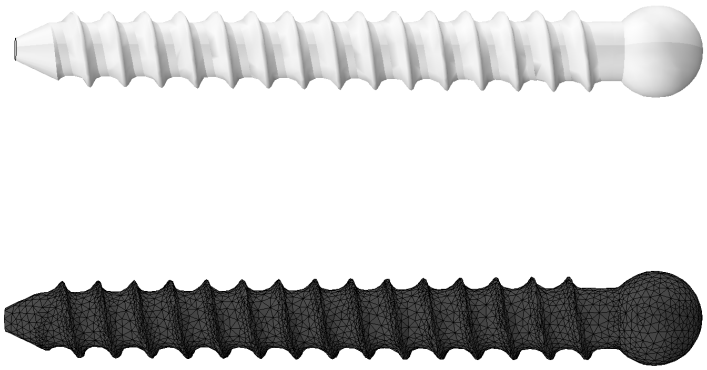

Figure 4.14: Modelled pedicle screw (top) with the FEM (bottom).

Having all the above into account, the selected screws have 5.5 mm of diameter and 45 mm of length.

Firstly one screw with those dimensions was modelled in *SolidWorks*, figure 4.14 (top), replicated five times, further rightly positioned on the respective vertebra (as explained in next section) and finally, meshed in the *Abaqus/CAE* software, figure 4.14 (bottom). The six pedicle screws have 46078 four-node tetrahedral elements (C3D4), table 4.9.

Once the screws were placed, each one was posterior connected with a rod, summing a total of four rod sections. Later these were meshed with B31 beam elements, in a total of 6 elements, 2 nodes each, 4.9. A beam structure is ideal for replicating a reliable rod since the beam elements resist bending, offering resistance to the loads applied during motion. These beams have a diameter of 5.5 mm and orientation, which corresponds to their tangent.

Table 4.9: PSS screws and rods' number of elements

Instrument	*Number of Elements*	*Diameter [mm]*	*Elements' Type*
Screws	46078 x6	N/A	C3D4
Rods	1 x4	5.5	B31

4.3.1.2 Vertebrae

The vertebrae without any screws were maintained intact. The three that are required for the treatment had firstly to be prepared for the screw insertion. This preparation was simply the extraction of the volume of the screws in their final position.

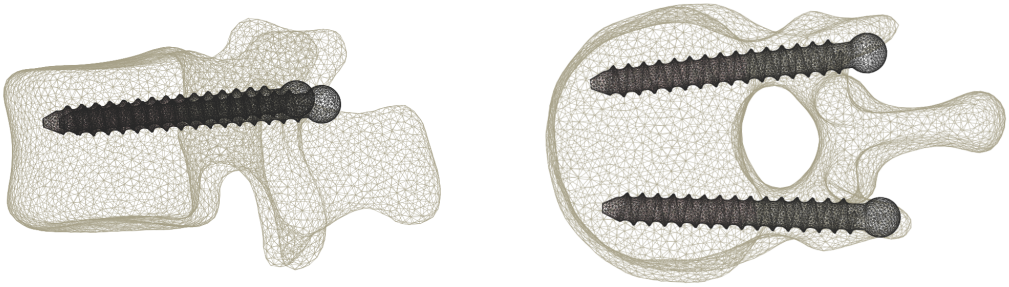

Figure 4.15: Pedicle screws axial (left) and sagittal (right) position.

This positioning and further subtraction was performed in the *Rhinoceros 6.0* software. As exemplified by figure 3.7 and subsection 3.3.3 of chapter 3, first a parallel plane to the superior endplate was created, which provides a biomechanic benefit [68]. This plane then intersected with the inferior edge of the transverse process, for T12, or with the mid of the transverse process for the lumbar L1 and L2 vertebrae. This plane region can be visually understood in figure 4.15 (left).

Since the entry point (posteriorly) of the screws is the intersection between the last axial plane and the superior articular facet for thoracic or the mamillary process for the lumbar, two sagittal planes on each side of the vertebra were created on that point.

To finalize the positioning direction, there was the need to create an angle from the outer cortical plane to the sagittal middle section, which allowed the two screws to converge and was not greater than 45º [69]. The pedicle is different for each vertebra, with the software help, this angle determination was easier due to the screw align with the pedicle, left axial view in figure 4.15.

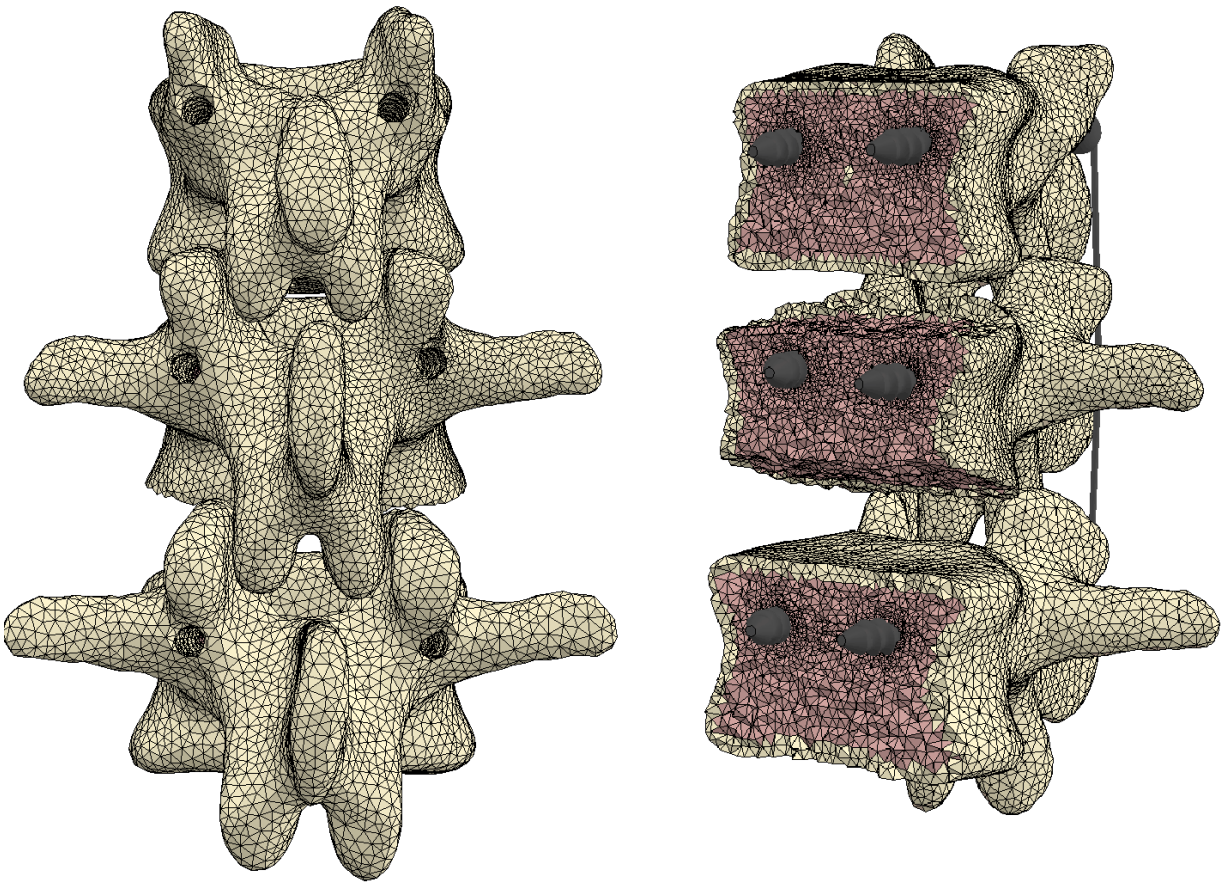

Figure 4.16: Fixed T12, L1 and L2 vertebrae posterior view (left) and with screws and rods anterior view with a coronal cross-section (right).

Along the same lines as the other two models, these vertebrae have then been meshed in four-node tetrahedral elements (C3D4), figure 4.16. In table 4.10, the only elements that are different from any so far are the T12, L1 and L2 elements, since they have a different structure. The screws have a complex structure, therefore their mirror in the vertebra are as well complex, leaving smaller elements around those areas. Despite the volume diminishment, the number of elements is higher, especially in the trabecular region, which has a bigger screw crossing.

Table 4.10: PSS vertebrae's number of elements

Vertebrae	*Cortical*	*Trabecular*	*Total*	*Elements' Type*
T11	35592	24343	59935	C3D4
T12	91473	113815	205288	
L1	110624	118439	229063	
L2	94633	115053	209686	
L3	55066	19382	74448	

4.3.1.3 PSS FEM full model

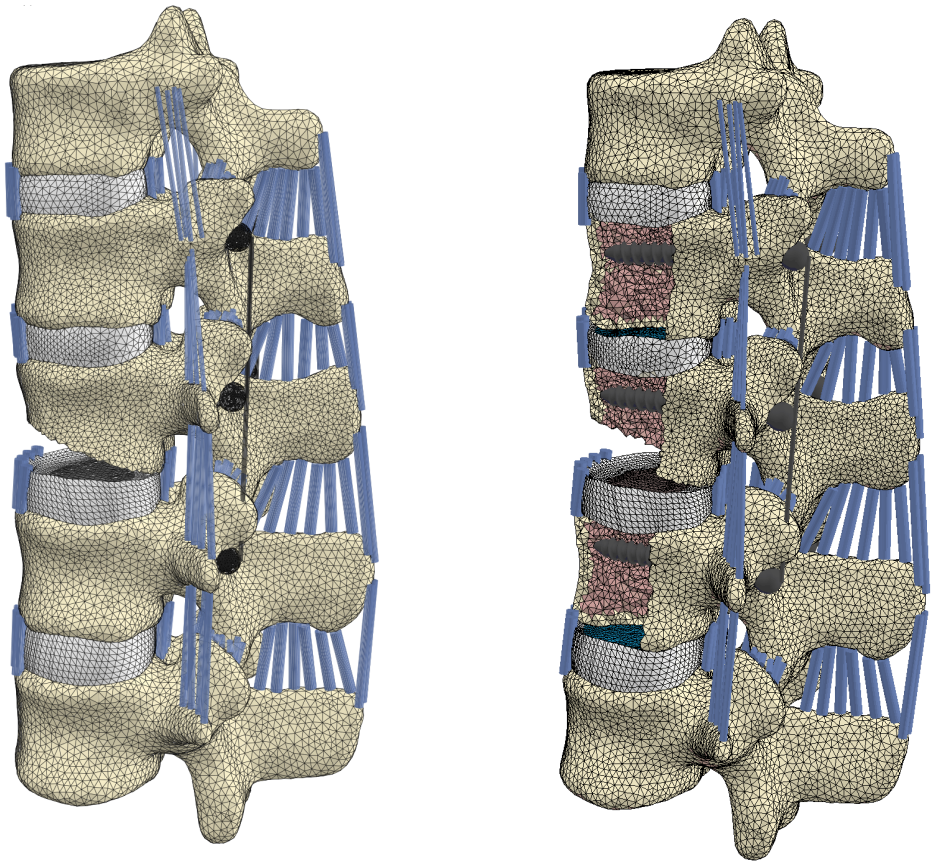

(a) Lateral view

(b) Lateral view with cuts

Figure 4.17: FE Posterior Short Segment Fixation with Intermediate Screws Model.

Figure 4.17 shows the lateral views of the complete PSS modelling model. In figure 4.17a is visible the rods and screw heads, and the complete burst fracture. Whereas, the cuts on figure 4.17b show the screw length.

4.3.2 Mechanical Properties

As the only new parts are the screws and the rods, their material properties were added to the elastic properties, table 4.11. Both are titanium alloys that have good biological and mechanical compatibility with human bones [70], with Young Modulus (E) = 110000 MPa and Poisson Ratio (υ) = 0.3 [71, 72].

Table 4.11: Screws and rods elastic mechanical properties

Elastic Component	Properties		Ref.
	Young Modulus (E) [MPa]	Poisson Ratio (υ)	
Screws and Rods	110000	0.3	[71, 72]

4.3.3 Contact Conditions

To fixate the screws on each vertebra, it was created a tie contact between the exterior screw surface and the inner vertebra holes surfaces, where the screws lay.

Comparably to the load surface, each screw head nodes' degrees of freedom were constrained to the respective rode node, using the kinematic coupling.

All the other boundary and contact conditions stayed the same, i.e., the tie constrains between the vertebrae's nodes and the ligaments' nodes between the intervertebral discs and the vertebral endplates; the inferior L3 vertebral endplate fixation and the superior T11 endplate load application of 5 Nm.

4.4 Posterior Long Segment Fixation Model

The *Posterior Long Segment Fixation* (PL) approach uses four vertebrae, different from the previous. They are the T11, T12, L2 and L3, leaving the L1 as is in the complete burst fracture model.

The process to obtain the PL model was similar to the PSS model, only changing the vertebrae above mentioned.

4.4.1 Components Modelling

4.4.1.1 Pedicle screws and rods

The positioning process of the screws on the T11 and T12 vertebrae is equal to the PSS T12 screw positioning. Whereas the L2 and L3 screws palecent is equivalent to the PSS L1 and L3 vertebra.

The screws elements are 46078 four node tetrahedral elements (C3D4), but this time multiplied by 8 since there are eight screws (2 screws x 4 vertebrae), table 4.12.

On the other hand, the rods follow the screws (figure 4.19), every rod has one linear line element of type B31 with two nodes. In total, 6 elements with 5.5 mm of diameter, table 4.12.

Table 4.12: PS screws and rods' number of elements

Instrument	*Number of Elements*	*Diameter [mm]*	*Elements' Type*
Screws	46078 x8	N/A	C3D4
Rods	1 x6	5.5	B31

4.4.1.2 Vertebrae

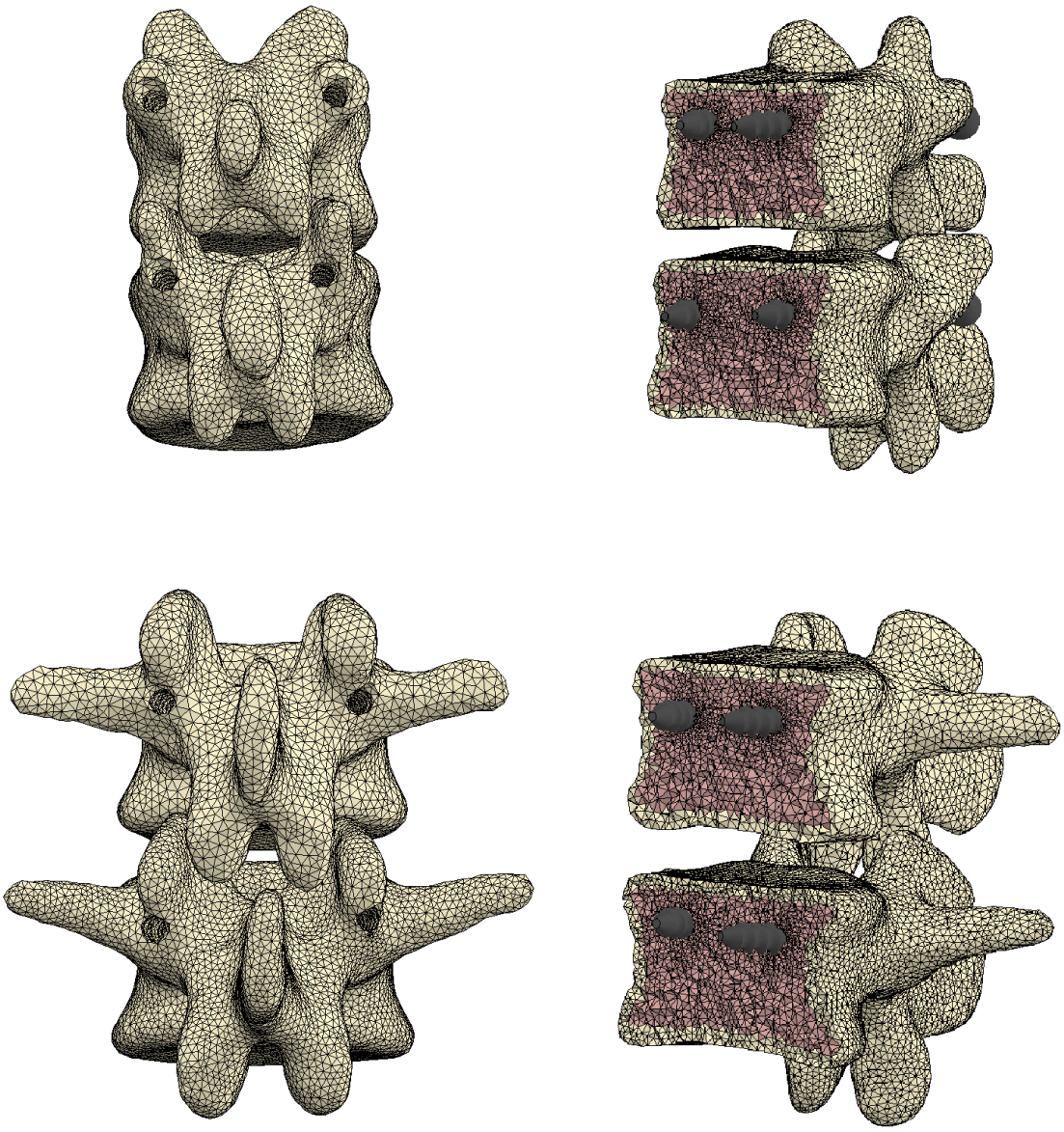

Figure 4.18: Fixed T11, T12, L2 and L3 vertebrae posterior view (left) and with screws anterior view with a coronal cross-section (right).

The process to achieve the T11, T12, L2 and L3 vertebrae shown in figure 4.18 was repeated from PSS model, and the L1 from the complete burst fracture model. Thus, the C3D4 element values of each region on table 4.13 are the same as the correspondent regions on tables 4.10 and 4.7.

Table 4.13: PL vertebrae's number of elements

Vertebrae	*Cortical*	*Trabecular*	*Total*	*Elements' Type*
T11	82007	103513	91473	
T12	91473	113815	205288	
L1	31805	11372	62344	C3D4
L2	94633	115053	209686	
L3	191808	136475	328283	

4.4.1.3 PL FEM full model

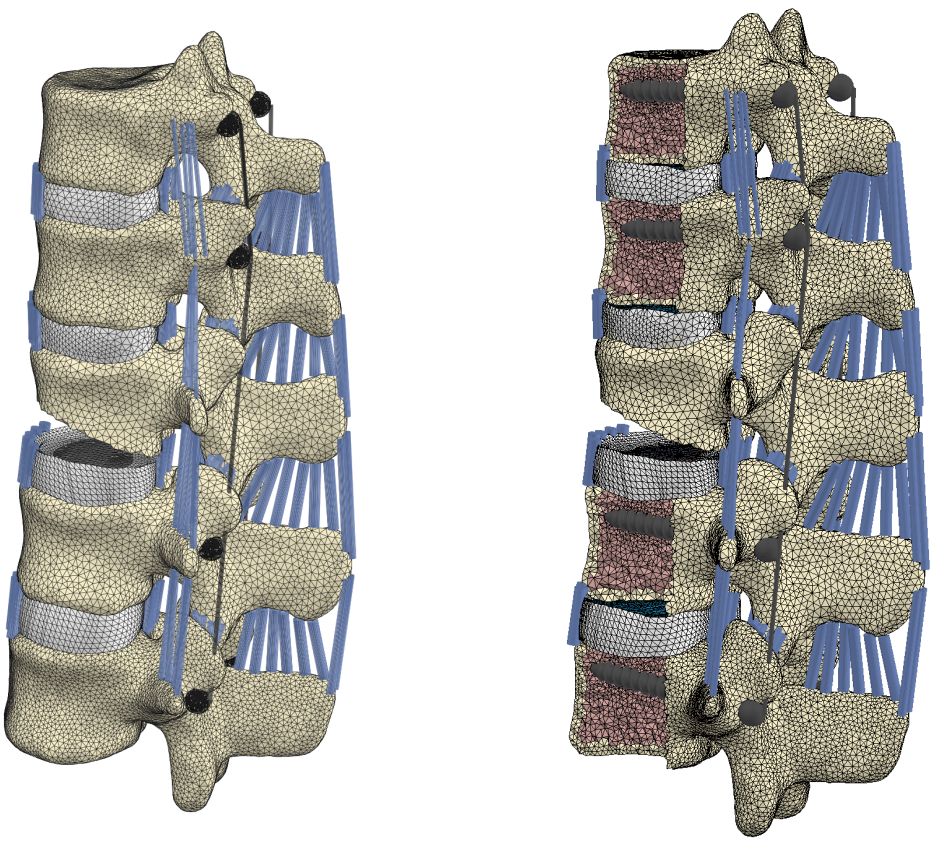

(a) Lateral view

(b) Lateral view with cuts

Figure 4.19: FE Posterior Long Segment Fixation Model.

Figure 4.19 shows the lateral views of the complete PL modelling model. In figure 4.19a is visible the rods and screw heads, and the complete burst fracture. Whereas, the cuts on figure 4.19b show the screw length.

4.4.2 Contact Conditions

All the contact conditions are similar to the PSS model. However, the differences rely on the position of the vertebrae holes and screws, in the T11, T12, L2 and L3, therefore, the same tie contact was applied in these four vertebrae and their screws.

Chapter 5

Results Analysis and Discussion

This chapter discriminates and further examines the results in four motions: flexion, extension, lateral bending and axial rotation, from the different models, whose load applied in the T11 superior vertebrae endplate corresponds to 5 Nm.

Firstly, it is addressed the validation of the intact model, which consists of its comparison between the *in vitro* bibliography values within the T11-L3 functional segments regions.

Secondly, the motion results' comparison between the previous and the pathological model is disclosed.

Finally, the two PSS and PLL fixation models' results are separately introduced and analysed. Further on, these get to be compared in terms of the total displacement, according to the fractured model variance. This stage leads to the conclusion of this dissertation, which aims to determine the most stable fixation model of the thoracolumbar spine.

5.1 Model Validation

As explained in subsection 4.1.5, it was applied a 5 Nm load in the T11 superior endplate of the intact model and further simulation for the flexion, extension, lateral bending and axial rotation motions. These were all simulated in the same conditions. The only difference resided in the momentum direction. Later the displacement results of each functional unit from T11 to L3 were calculated.

The results are measured in Range of Motion (ROM), expressed in angular degrees (º), i.e., the diverse functional units' angular displacement difference between the model with no load applied and its full motion with the maximum 5 Nm load.

The ROM values were obtained by calculating the angle between the two vectors of each vertebra, in radians, and posteriorly transformed into degrees, equation 5.1, using equation 5.2:

$$\Theta = \arccos(< \overrightarrow{AB_1}, \overrightarrow{AB_2} >) \quad rad \quad = \quad \left(\frac{180\Theta}{\pi}\right)^{\circ} \tag{5.1}$$

where,

$$< \overrightarrow{AB_1}, \overrightarrow{AB_2} >= \cos\Theta . \left|\overrightarrow{AB_1}\right| . \left|\overrightarrow{AB_2}\right| \tag{5.2}$$

These vectors were determined given two points of the vertebra, equation 5.3, one located on the surface of the superior vertebral endplate and the second on the surface of the inferior endplate.

$$\overrightarrow{AB} = (x_B - x_A, y_B - y_A, z_B - z_A) \tag{5.3}$$

Every ROM angle of the intact T11-L3 model is displayed in table 5.1 by motion and functional unit (region) from T11 to L3.

In the flexion motion, the T12-L1 functional unit displacement is the highest with 2.52º, corresponding to the dorsolumbar transition, i.e., the transition from a stiffer region to a more flexible one. It is lower in the thoracic region (T11-T12) with a 1.74º displacement. However, the T11-T12 present a higher extension ROM of 2.18º, followed by the 2.10º of L2-L3, 1.72º of L1-L2 and T12-L1 with 1.07º. The lateral bending ROMs are the ones where the difference between values is the smallest, corresponding to 0.3º of maximum difference. The higher axial rotation ROM corresponds to the T11-T12 and the lowest to the followed functional unit. The two last regions are similar and have 2.10º and 2.19º respectively.

Table 5.1: Intact model ROM results

Region	*Flexion ROM [º]*	*Extension ROM [º]*	*Lateral Bending ROM [º]*	*Axial Rotation ROM [º]*
T11-T12	1.74	2.18	1.70	4.97
T12-L1	2.52	1.07	1.70	1.03
L1-L2	2.10	1.72	1.90	2.10
L2-L3	2.32	2.10	2.00	2.19
T12-L2 Sum	4.62	2.79	3.60	3.13
T11-L3 Sum	8.89	7.07	7.30	10.29

The validation is necessary to authenticate the credibility of the results obtained [25]. Therefore, the values in table 5.1 were correlated with experimental results.

In this case, the intact model results for the flexion, extension, lateral bending and axial rotation motions generated by a load of 5 Nm applied on the centre point of the T11 superior vertebral endplate are correlated with the *in vitro* results retrieved from Yamamoto *et al.* (1989) [73] with a 10 Nm load, Oxland *et al.* (1992) [74] with a 7.5 Nm load, Marien *et al.* (2017) [75] with a 5

Nm load and Busscher *et al.* (2011) [76] with a 4 Nm load. Each momentum validation results are illustrated from figure 5.1 to figure 5.4.

Despite the differences in the load's magnitudes and their non-linear correlation to the motion, these allow a validation on a bigger scope, since the intact model can be directly compared with the Marien *et al.* (2017), verified if its values are not higher than Yamamoto *et al.* (1989) or Oxland *et al.* (1992) nor lower than Busscher *et al.* (2011). The functional units (regions) of the model are T11-T12, T12-L1, both not present in Oxland *et al.* (1992), L1-L2 and L2-L3, both not present in Yamamoto *et al.* (1989).

The flexion motion comparison between the cadaveric references and the intact model is represented in figure 5.1. It shows a slight stiffness in the region T12-L1 compared with the same pure moment, and slightly more flexible than the L1-L2 and L2-L3 cadaveric functional units, being within the data range.

On the other hand, the extension motion is opposite to the flexion. This model's T11-T12 and L2-L3 regions are stiffer than the matched momentum reference (figure 5.2).

Despite the T11-T12 lower lateral bending motion ROM (figure 5.3) compared with the other 5 Nm motion, this last is higher the higher motion, showing a nonlinear behaviour. Therefore, this example shows the advantage of having a range of momentums. Whereas, the other regions are within the scope of the 5 Nm momentum.

Lastly, the axial rotation motion major values, shown in figure 5.4, are correlated with the cadaveric ROM values.

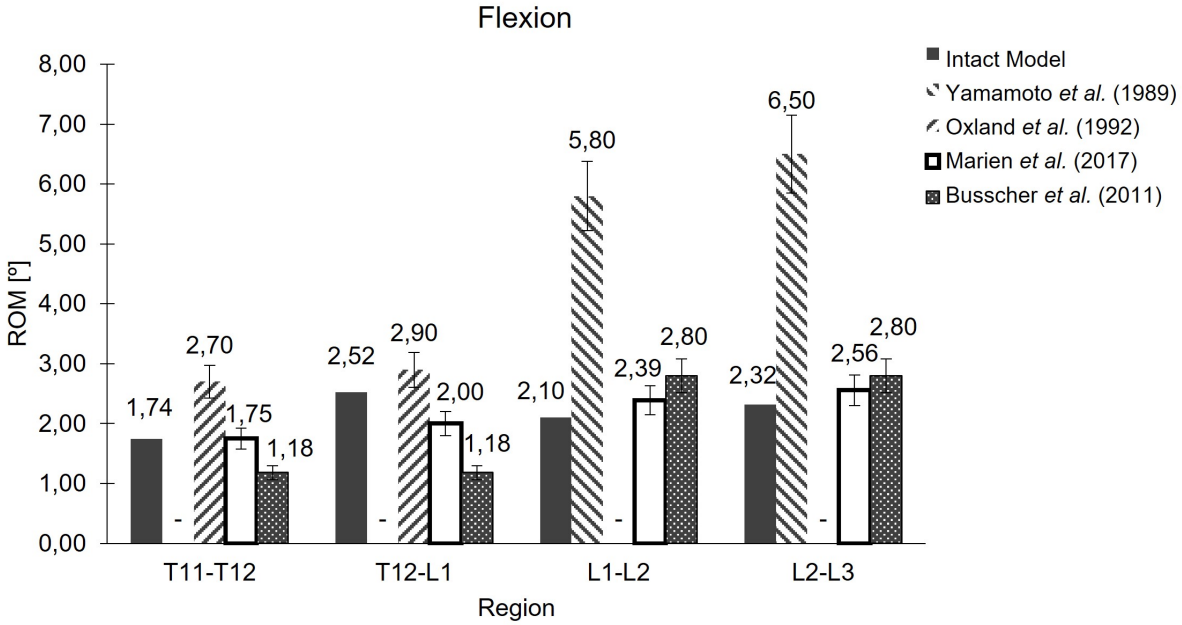

Figure 5.1: Comparison of the ROM results for the flexion motion of the intact model with a load of 5 Nm between the Yamamoto *et al.* (1989) with a 10 Nm load, Oxland *et al.* (1992) with a 7.5 Nm load, Marien *et al.* (2017) with a 5 Nm load and Busscher *et al.* (2011) with a 4 Nm load.

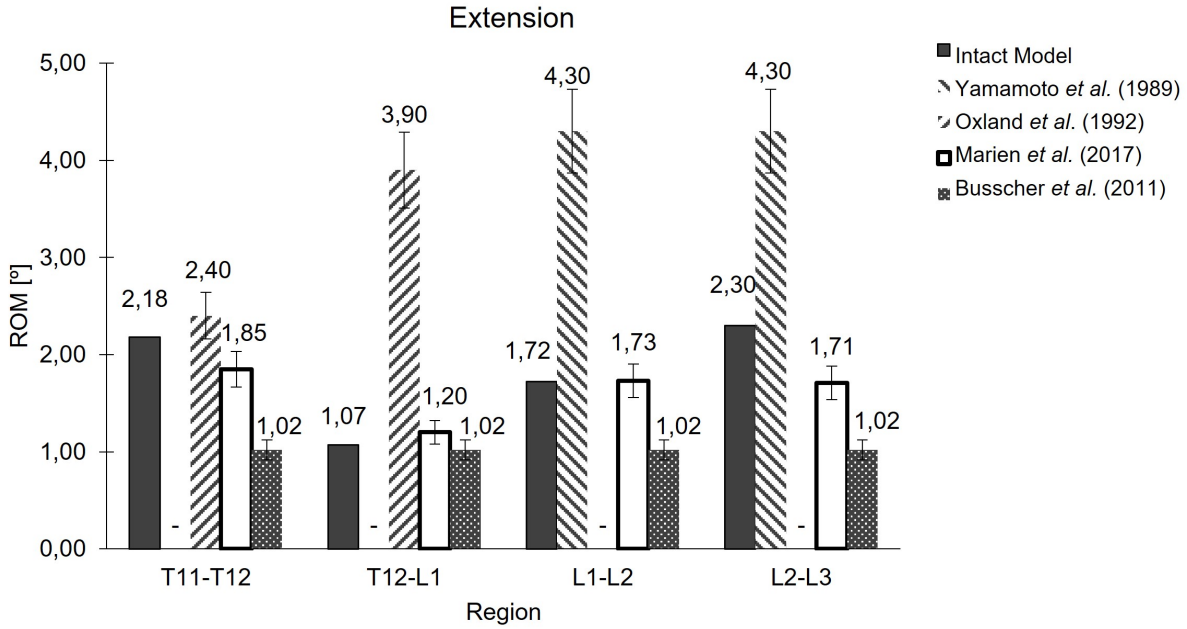

Figure 5.2: Comparison of the ROM results for the extension motion of the intact model with a load of 5 Nm between the Yamamoto *et al.* (1989) with a 10 Nm load, Oxland *et al.* (1992) with a 7.5 Nm load, Marien *et al.* (2017) with a 5 Nm load and Busscher *et al.* (2011) with a 4 Nm load.

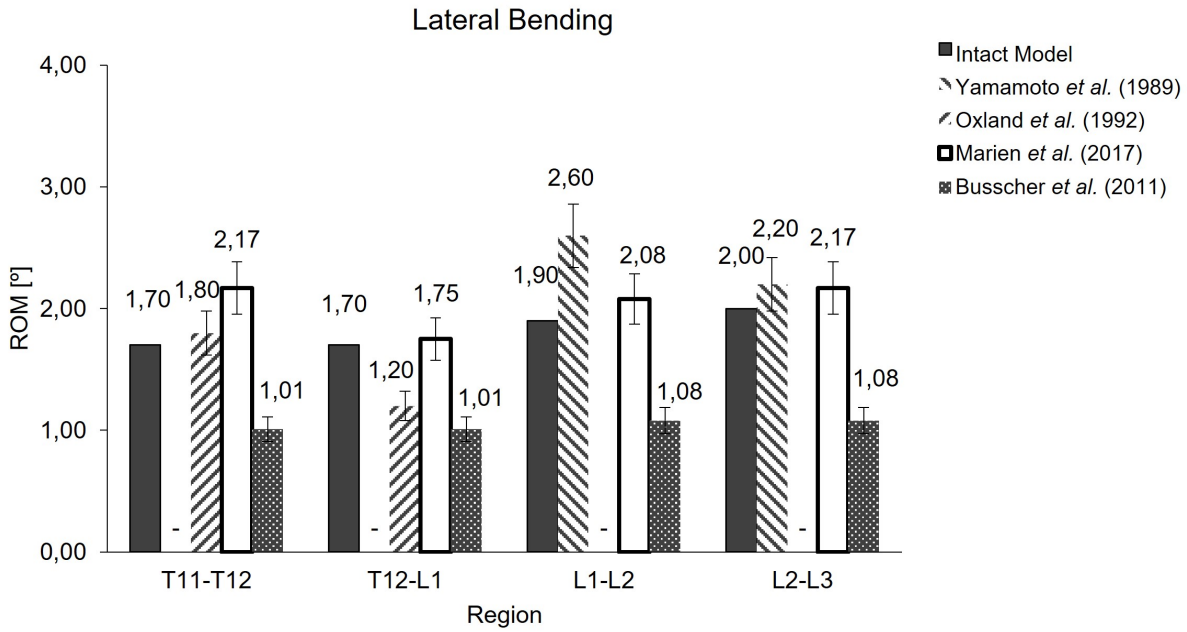

Figure 5.3: Comparison of the ROM results for the lateral bending motion of the intact model with a load of 5 Nm between the Yamamoto *et al.* (1989) with a 10 Nm load, Oxland *et al.* (1992) with a 7.5 Nm load, Marien *et al.* (2017) with a 5 Nm load and Busscher *et al.* (2011) with a 4 Nm load.

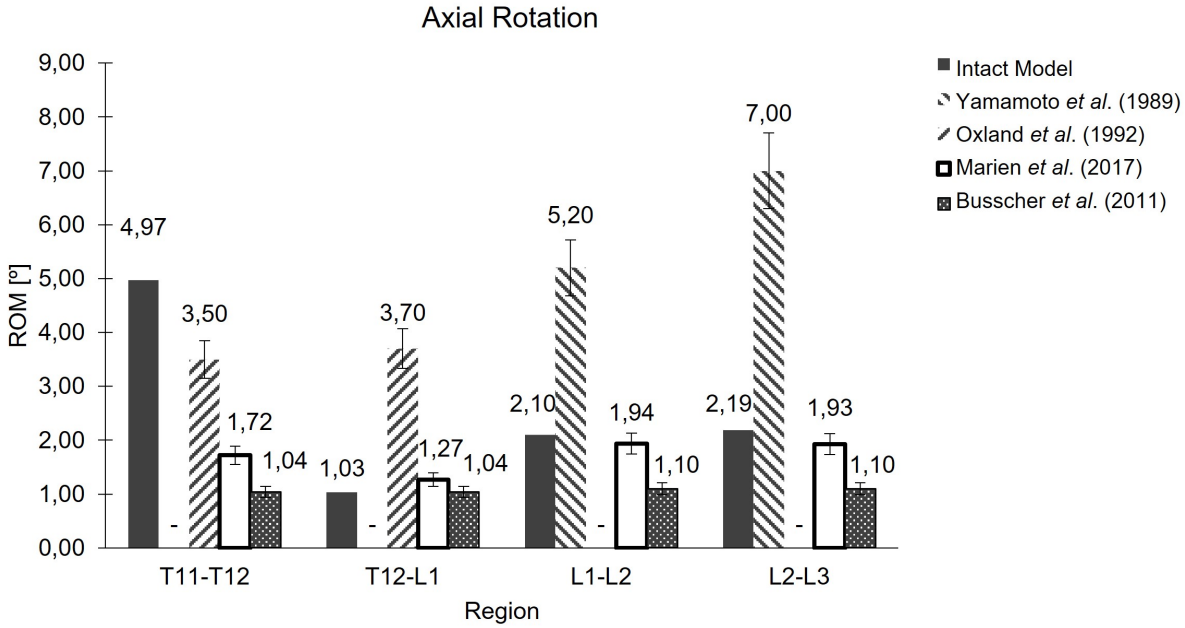

Figure 5.4: Comparison of the ROM results for the axial rotation motion of the intact model with a load of 5 Nm between the Yamamoto *et al.* (1989) with a 10 Nm load, Oxland *et al.* (1992) with a 7.5 Nm load, Marien *et al.* (2017) with a 5 Nm load and Busscher *et al.* (2011) with a 4 Nm load.

The previously described motions' ROM of the intact dorsolumbar model and respective correlation with bibliographic retrieved experimental values entail a proper validation of the model. Hence, the other models' simulations could have proceeded with the same properties and conditions, whose values can be further conferred.

5.2 Complete Burst fracture Model

In the complete burst fracture model, the 5 Nm loads for the flexion, extension, lateral bending and axial rotation were applied and their output further analysed.

As previously, the results were calculated using the equations 5.1 and 5.2 for the T11-T12, T12-L1, L1-L2 and L2-L3 domains. This step is important to compare the complete burst model ROM values with the intact model ROM values and verify the larger movements of the first model.

Looking at the tables 5.2 and 5.1, the bulk of the burst ROM values are higher than the intact ones. Except for the flexion and lateral bending motion on the T11-T12 and L2-L3, the reason being the low resistance of the broken L1 vertebra, thus the T12-L1 and L1-L2 flexion and lateral bending ROM are higher in the burst model than the intact model. In all the motions, these two regions have greater ROM values, due to the lack of rigid bone, which allows larger mobility.

Table 5.2: Complete burst model ROM results

Region	*Flexion ROM [°]*	*Extension ROM [°]*	*Lateral Bending ROM [°]*	*Axial Rotation ROM [°]*
T11-T12	1.73	2.26	1.52	7.14
T12-L1	4.02	11.09	6.09	50.01
L1-L2	3.24	16.81	6.37	33.67
L2-L3	1.89	2.60	1.78	2.17
T12-L2 sum	7.26	27.90	12.46	83.69
T11-L3 sum	10.89	32.75	15.76	93.00

Analysing only the table 5.2 with the ROM values, it is possible to correlate them with figure 5.5 for the corresponding motions. Each subfigure is colour-coded according to the displacement of the nodes (U, Magnitude) in mm. For a better overall understanding and latter usage, each region value was added to the ones for the same motion. First from the T12 to L2 functional unit, which will be used to compare with the PSS results since this is the scope of interest. At last, the sum from T11 to L3 functional units, the same regions of interest for PL and current models.

In the first motion, flexion, the larger angle is between the T12 and L1 vertebra, 4.02º, followed by the L1-L2 segment with 3.24º. As expected, these two areas are the most affected by the 5 Nm load since it is the burst site. Both ends of the total model segment have similar small ROM, 1.89º in L2-L3 and 1.73º in the T11-T12 unit.

The extension ROM values are higher than the flexion ROM. The weaker ALL ligaments that operate in the extension motion and the largest region of flexible vertebral body elements (subsection 4.2.2) allocated in the anterior lower portion of the vertebra justify those results. The lower part being less rigid promotes the highest ROM of 16.81º in the T2-L1 column segment, followed by the T12-L1 with 11.09º. The remnant functional units have lower ROM with 2.60º in the last functional unit and 2.16º in the first.

The overall lateral bending ROM succeeds the flexion values because the model' ligaments that take effect on this motion were not changed. However, the two centre functional units are still more flexible, leading to higher values of 6.37º (L1-L2) and 6.09º (T12-L1). Once again, the T11-T12 and L2-L3 have proximate ROM of 1.52º and 1.78º, respectively.

Lastly, the motion that has the highest values in the burst region is the axial rotation, like in the validated model, with the distinction of the changed ALL and vertebral body elements. That affects the axial flexibility, leading to the highest rotations on the T12-L1 and l1-l2, with 50.01º and 33.67º, respectively.

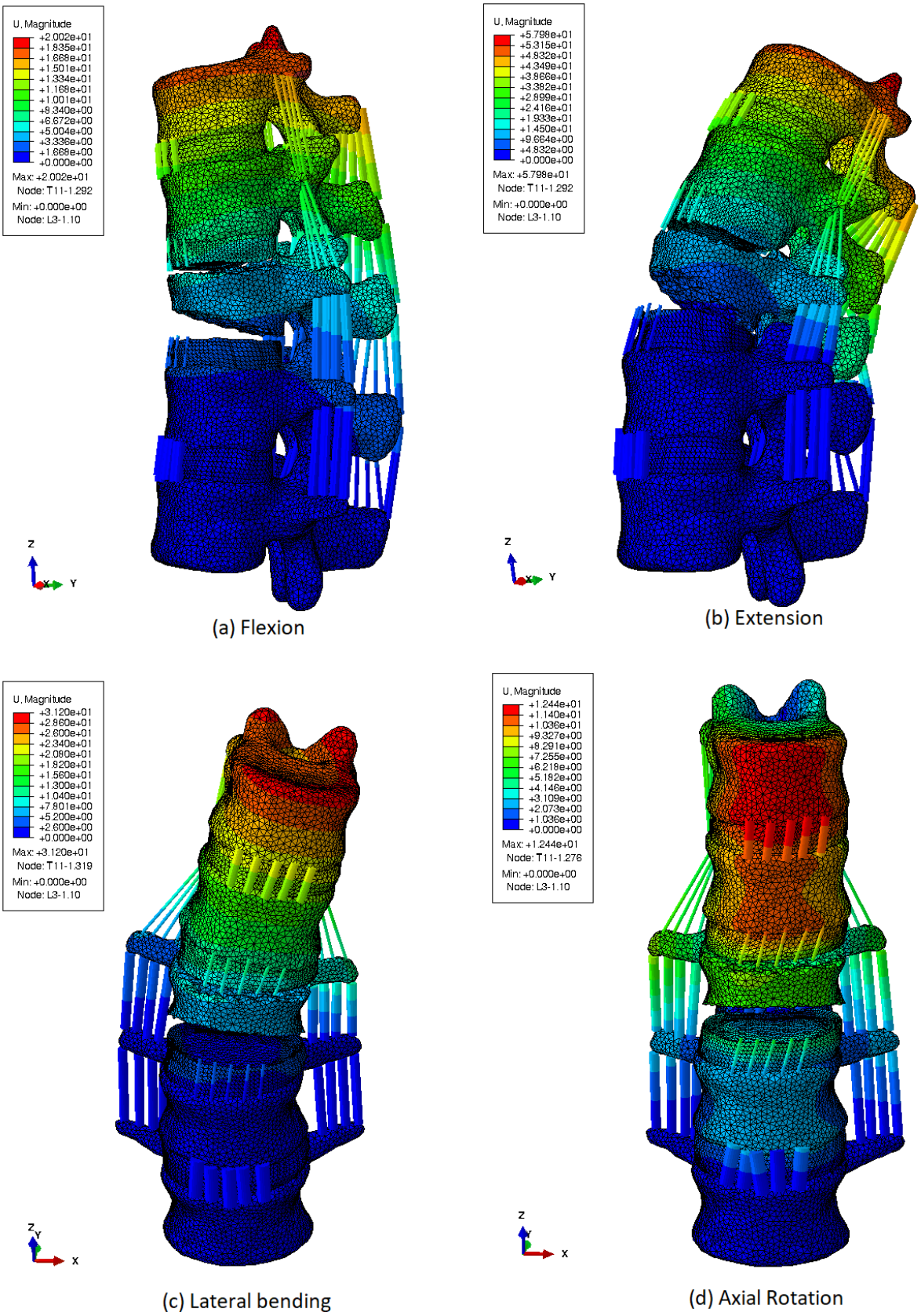

Figure 5.5: Colour-code displacement of the T12-L3 functional units of the complete burst FE model for the (a) flexion, (b) extension, (c) lateral bending and (d) axial rotation motions.

The total displacement indicates how much millimetres the nodes dislocated. In figure 5.5 is possible to visualize the position state of the dorsolumbar vertebral segment after a 5 Nm load application. The node which represents the sum of the displacements is always located in the T11 vertebra. Both flexion and extension motions share the same representative node, located in the T11 superior articular facet. The maximum displacement node in the lateral bending motion in the same facet, whereas the node in the axial rotation belongs to the anterior portion of the t11 body. All four motions have a minimum displacement on the lower fixated node.

Epitomising, the ROM is calculated between each vertebra, leading to higher values in the problematic zones, i.e., where the L1 fractured vertebra is found. Whilst the displacement is the sum of each vertebra's displacement, registering always the highest in the T11 vertebra.

5.3 Posterior Short Segment Fixation with Intermediate Screws Model

Since the PLL model only fixates the T12-L1 and L1-L2 segments, the ROM was only calculated in these two functional units. Therefore, those values are discriminated in table 5.3 for each motion after a 5 Nm load.

Table 5.3: PSS fixation model ROM results

Region	*Flexion ROM [º]*	*Extension ROM [º]*	*Lateral Bending ROM [º]*	*Axial Rotation ROM [º]*
T12-L1	0.72	0.87	3.88	32.29
L1-L2	1.96	3.54	0.25	12.74
Sum	2.69	4.40	4.13	45.03

The lower sum of ROM happens in the flexion motion. The T12-L1 has 0.72º, followed by the 1.96º of L1-L2.

The lateral bending succeeds the previous with a total of 4.13º. However, the smallest ROM is found in this motion on the L1-L2 vertebra with 0.25º coupled with the T12-L1 3.88º of ROM.

The Extension is alongside the lateral bending with a difference of 0.27º. Here the highest values reside on the L1-L2 segment with 3.54º, joined with the 0.87º in the first segment.

The highest ROM values occur in the axial rotation, with a 32.29º and 12.74º of ROM from up-down. The rods allow slight torsion freedom since they have bending resistance due to their properties (section 4.3) but can rotate around their vertical axis.

By analysing the figure 5.6 it is possible to visualize the motion's final position and associate them with the ROM values. The notorious T12-L1 and L1-L2 deviated ALL correlates with the biggest axial rotation ROM angle.

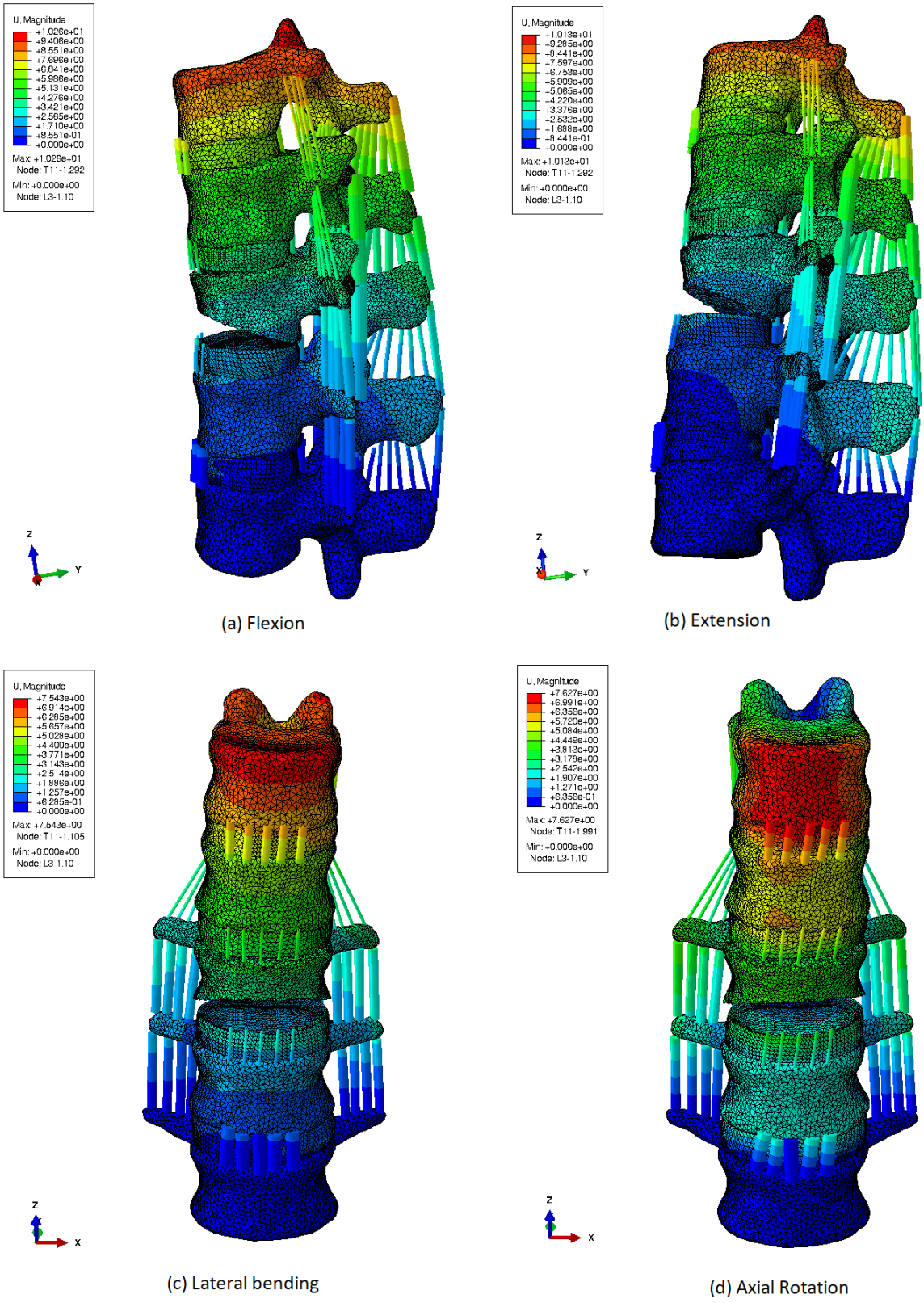

Figure 5.6: Colour-code displacement of the T12-L3 functional units of the Posterior Short Segment Fixation with Intermediate Screws FE model for the (a) flexion, (b) extension, (c) lateral bending and (d) axial rotation motions.

5.4 Posterior Long Segment Fixation Model

The *Posterior Long Segment Fixation Model* (PL) has all four functional units (from T11 to L3) fixed. Even though the L1 vertebra has no pedicle screws, its movement is restrained by the adjacent fixated vertebrae. The respective ROM values can be seen in table 5.4 and supported by the figure 5.7.

Table 5.4: PL fixation model ROM results

Region	*Flexion ROM [º]*	*Extension ROM [º]*	*Lateral Bending ROM [º]*	*Axial Rotation ROM [º]*
T11-T12	0.15	0.13	0.05	3.62
T12-L1	1.00	0.56	0.01	23.25
L1-L2	0.79	0.90	0.37	25.29
L2-L3	0.32	0.12	0.10	0.25
Sum	2.27	1.71	0.53	52.41

In the PL model, the lower set of ROM values refer to lateral bending. This motion has 0.01º in the T11-T12, 0.05º in T12-L1, 0.10º in L2-L3 and 0.37º in L1-L2.

The extension ROMs are not as smaller as the previous ones but are still under 1º. The two middle section functional units have the largest ROM of 0.90º and 0.56º. The T11-T12 and L2-L3 regions have closer values with one another of 0.13º and 0.12º, respectively.

The flexion motion follows the extension motion in what concerns the ROM values. Here the same aspect of the middle section is observed, T12-L1 and L1-L2 functional units have haver values, with 1.00º and 0.79, respectively. The T11-T12 unit has 0.15º of ROM, wheres the L2-L3 presents 0.32º.

Finally, as analysed in the PS model, the axial rotation has the highest values of all motions, especially in the T12-L1 and L1-L2, with 23,25º and 25.29º. Antagonicaly, the T11-T12 and L2-L3 rotated 3.62º and 0.25º, respectively.

The displacement is shown in figure 5.7, whose maximum for the flexion and extension motions is in the T11 superior articular facet. Both lateral bending and axial rotation have their maximum in the anterior upper portion of the T11 body.

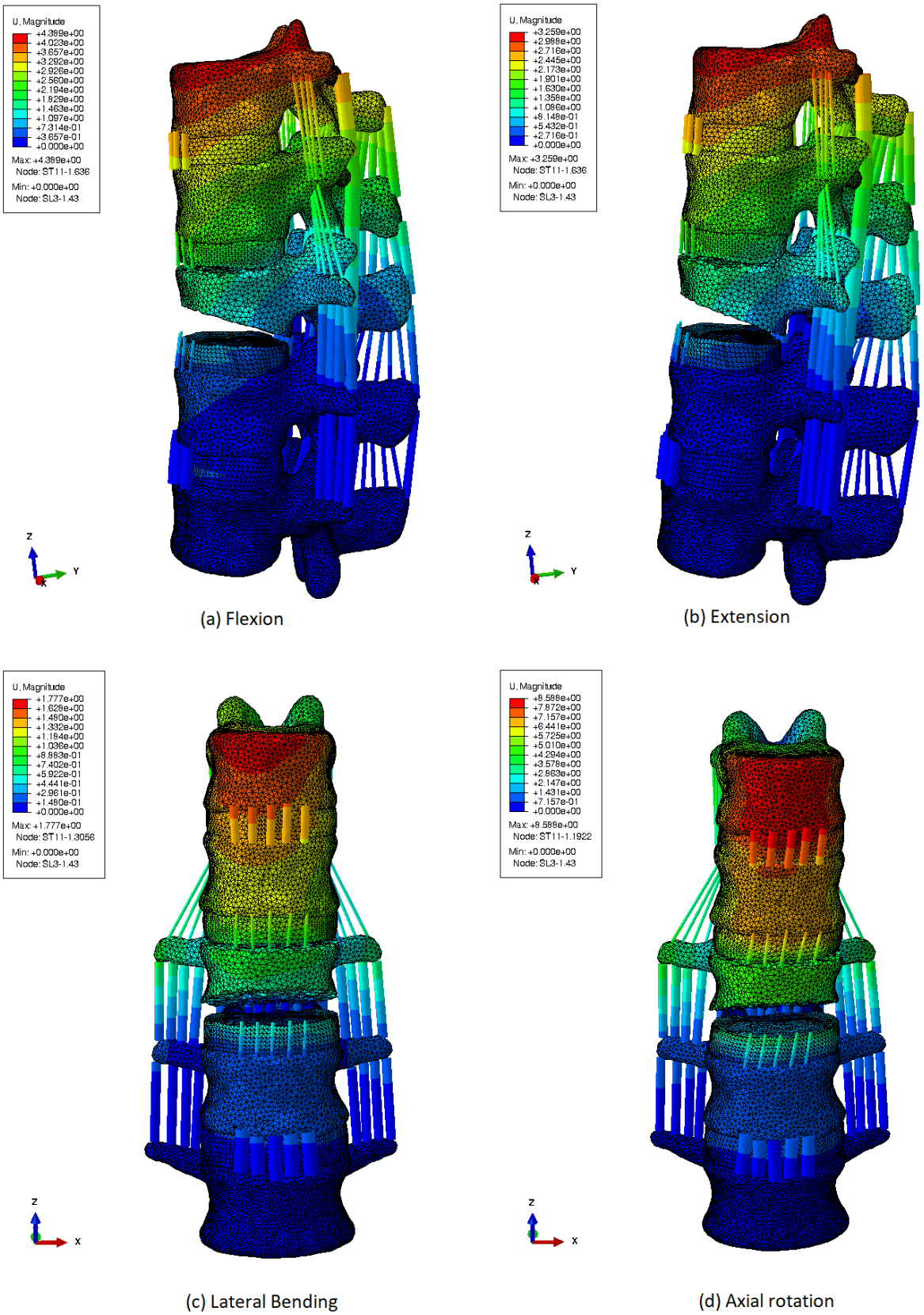

Figure 5.7: Colour-code displacement of the T12-L3 functional units of the Posterior Long Segment Fixation FE model for the (a) flexion, (b) extension, (c) lateral bending and (d) axial rotation motions.

5.5 Posterior fixation models' benchmarking

After obtaining the intact, complete burst, *Posterior Short Segment Fixation with Intermediate Screws* and *Posterior Long Segment Fixation* models ROM results, it is possible to combine the data and compare the biomechanical behaviour of the two fixation models. Since it would be mindless to compare the two fixed functional units of PSS with the four of the PL, both require results handling. With the difference with the intact model (intact model sum minus the PSS/PL sum), it is possible to understand which posterior fixation model behaviour is closer to the intact healthy model. Closer to the absolute result to zero, closer to the intact model. Whilst the difference with the complete burst model (burst model sum minus the PSS/PL sum) depicts the stiffness of the treatments. Broader the difference, less flexible is the fixation model. All these values are discriminated in table 5.5.

Table 5.5: Comparison between PSS and PL models

Posterior Fixation Model Relation	*Flexion ROM [°]*	*Extension ROM [°]*	*Lateral Bending ROM [°]*	*Axial Rotation ROM [°]*
Intact - PSS	1.93	-1.61	-0.53	-41.90
Intact - PL	6.62	5.36	6.77	-42.12
Burst - PSS	4.58	23.50	11.94	38.66
Burst - PL	8.62	31.05	15.23	40.58

Comparing the fixation models through their approximation to the intact models, the PSS ROM values are closer in every motion, with a difference of 0.53º in the lateral bending, 1.61º in extension, 1.93º less than in the intact (only positive) value for flexion and with a larger angle in the axial rotation, of 41,9º. However, in the last motion, the PL difference is almost the same as the PSS, with more 42,12º than the intact model. It is the only value that exceeds the reference one. In the flexion, extension and lateral bending, the range of motion is always less than the intact model, with a difference of 6.62º, 5.36º and 6.77º, respectively.

Lastly, in table 5.5 it is also presented the difference with the burst model, where can be concluded that the PL model is furthest from the unstable pathological model in the positive direction, i.e., the more stable model. The PSS is closer 4.58º, 23.50º, 11.94º and 38.66º to the burst model in flexion, extension, lateral bending and axial rotation, respectively. Adversely, it can be stated that the PL 8.62º, 31.05º, 15.23º and 40.58º afar from the reference model, in flexion, extension, lateral bending and axial rotation, respectively.

All in all, the *Posterior Long Segment Fixation* model has less movement freedom, being more steady than the *Posterior Short Segment Fixation with Intermediate Screws* model.

5.6 Final Considerations

The presented results are specific for the dorsolumbar FE model, with the proviso that was not considered the spinal musculature which gives higher stability to the vertebral column, the surrounding soft tissues, as well as the rib cage which restricts the free movements in the thoracic region.

Chapter 6

Conclusions and Future Work

This dissertation on *Computational Study on the Dorsolumbar Compression Fracture and its Fixation Methods* successfully achieved its proposed goals.

The main objective was to obtain two comparable finite element dorsolumbar posterior fixation models and settle the most sturdy one. To that end, it was created a finite element intact healthy model of the T11-L3 vertebral column segment, followed by a similar model with the complete burst fracture (A4) L1 vertebra. Making use of the previous, the *Posterior Short Segment Fixation with Intermediate Screws* and *Posterior Long Segment Fixation* finite element models were modelled. Posteriorly, a load of 5 Nm was applied in all the FE models and the ROM was retrieved for the flexion, extension, lateral bending and axial rotation motions. The intact model ROM purpose relied on model validation. The burst model is the bridge for the two fixations methods comparison.

Despite all the differences, both methods result in similar maintenance of the sagittal alignment, kyphosis correction, neurological pain reduction and biomechanical behaviour factors as what concerns the bibliography research, but no differences for these two specific approaches were found. It was expected a very similar biomechanical behaviour in both. Results show that both models successfully fixate the segment of interest, and that the Posterior Long Segment Fixation model has less movement freedom, being more steady than the Posterior Short Segment Fixation with Intermediate Screws model. The PL approach is the best one as it yields to a stiffer spine segment. On the other hand, if the surgeon aims to reduce the spine movements, the PSS approach could be chosen, if the fracture is quite stable.

Throughout the methods used in this dissertation, it is concluded that the simulation with the finite element method is suitable for this type of studies implying the desirable body anatomy reconstruction, with no need for using cadaveric samples with the exact pathology, all the apparatus nor the need for putting voluntary patients through constant monitoring for the sake of the study. However, in order to make the numerical simulation executable, some aspects of the model need to be simplified, diverging from the human characteristics.

At last, it could be interesting to add the musculature, and the rib cage to the presented models, and further analyse the stress around the screw surface and each intervertebral discs comparing

them with both fixation methods alongside the already calculated ones. In addition, the intact healthy and pathological dorsolumbar finite element models are a starting point for other fixation methods or pathologies studies.

References

[1] Theo Vos and et al. Global, regional, and national incidence, prevalence, and years lived with disability for 328 diseases and injuries for 195 countries, 1990–2016: a systematic analysis for the global burden of disease study 2016. *The Lancet*, 390(10100):1211–1259, 2017.

[2] Narayan Yoganandan, Joel B Myklebust, Gautam Ray, and Anthony Sances Jr. Mathematical and finite element analysis of spine injuries. *Critical reviews in biomedical engineering*, 15(1):29, 1987.

[3] Wafa Skalli, David Mitton, Philippe Rouch, and Jean Dubousset. Biomechanics and spinal modelling. In *Spinal Anatomy*, pages 491–503. Springer, 2020.

[4] Martin Scaal. Seminars in Cell & Developmental Biology Early development of the vertebral column. *Seminars in Cell and Developmental Biology*, 49:83–91, 2016.

[5] John DeSesso. Vascular ontogeny within selected thoracoabdominal organs and the limbs. *Reproductive Toxicology*, 70, 10 2016. doi:10.1016/j.reprotox.2016.10.007.

[6] Sebastien Pesenti, Nicole Philip, and Gerard Bollini. Embryology of the vertebral column. In *Spinal Anatomy*, pages 19–24. Springer, 2020.

[7] Kevin M Kaplan, Jeffrey M Spivak, and John A Bendo. Embryology of the spine and associated congenital abnormalities. *The Spine Journal*, 5(5):564–576, 2005.

[8] Louay Kalamchi and Cristina Valle. Embryology, vertebral column development. In *StatPearls [Internet]*. StatPearls Publishing, 2019.

[9] Charisma DeSai and Amit Agarwal. Anatomy, back, vertebral column. In *StatPearls [Internet]*. StatPearls Publishing, 2018.

[10] Vishy Mahadevan. Anatomy of the vertebral column. *Surgery (Oxford)*, 36(7):327–332, 2018.

[11] A Dimeglio, F Bonnel, and F Canavese. The growing spine. In *Spinal Anatomy*, pages 25–52. Springer, 2020.

[12] Kevin K Haussler. Anatomy of the thoracolumbar vertebral region. *Veterinary clinics of North America: equine practice*, 15(1):13–26, 1999.

[13] VanPutte and *et al.* Coluna vertebral. In *Seeley's Essentials of Anatomy Physiology*. Mc Graw Hill Education, 2017.

[14] Alan Rawls and Rebecca E Fisher. Developmental and functional anatomy of the spine. In *The genetics and development of scoliosis*, pages 1–29. Springer, 2018.

[15] Valério Henrique Dezan. Análise do comportamento mecânico dos discos intervertebrais em diferentes faixas etárias. 2005.

[16] Eric Whitney and Anthony J Alastra. Vertebral fracture. 2019.

[17] Richard L. Drake and *et al.* Anatomia regional. In *Gray's Anatomia para Estudantes*. ELSEVIER, 2010.

[18] Brett Sassack and Jonathan D Carrier. Anatomy, back, lumbar spine. In *StatPearls [Internet]*. StatPearls Publishing, 2020.

[19] Nabil A Ebraheim, Ali Hassan, Ming Lee, and Rongming Xu. Functional anatomy of the lumbar spine. In *Seminars in pain medicine*, volume 2, pages 131–137. Elsevier, 2004.

[20] Robert J Kowalski, Lisa A Ferrara, and Edward C Benzel. Biomechanics of the spine. *Neurosurgery Quarterly*, 15(1):42–59, 2005.

[21] Reinhard Putz. The detailed functional anatomy of the ligaments of the vertebral column. *Annals of anatomy*, pages 40–47, 1992.

[22] Emily A Bermel, Victor H Barocas, and Arin M Ellingson. The role of the facet capsular ligament in providing spinal stability. *Computer methods in biomechanics and biomedical engineering*, 21(13):712–721, 2018.

[23] Kai-Uwe Schmitt, Peter F Niederer, Markus H Muser, and Felix Walz. *Trauma biomechanics: Introduction to accidental injury*. Springer Science & Business Media, 2013.

[24] Duane Knudson. Introduction to biomechanics of human movement. In *Fundamentals of Biomechanics*, pages 3–22. Springer, 2003.

[25] Márta Kurutz and László Oroszváry. Finite element modeling and simulation of healthy and degenerated human lumbar spine. *Finite Element Analysis: From Biomedical Applications to Industrial Developments*, page 193, 2012.

[26] William S. Marras. Biomechanics of the spinal motion segment | clinical gate. `https://clinicalgate.com/biomechanics-of-the-spinal-motion-segment/`. (Accessed on 07/06/2020).

[27] AA White and MM Panbaji. Clinical biomechanics of the spine. 1990.

[28] Vincent J Miele, Manohar M Panjabi, and Edward C Benzel. Anatomy and biomechanics of the spinal column and cord. In *Handbook of clinical neurology*, volume 109, pages 31–43. Elsevier, 2012.

[29] JJ Wortman and RA Evans. Young's modulus, shear modulus, and poisson's ratio in silicon and germanium. *Journal of applied physics*, 36(1):153–156, 1965.

[30] Nikolai Bogduk. *Clinical anatomy of the lumbar spine and sacrum*. Elsevier Health Sciences, 2005.

[31] António Miguel Cardia Melro Rodrigues. *Análise e projecto de estruturas para substituição do disco intervertebral*. PhD thesis, Faculdade de Ciências e Tecnologia, 2012.

[32] A Gloria, T Russo, R De Santis, and L Ambrosio. Composite materials for spinal implants. In *Biomedical composites*, pages 139–161. Elsevier, 2017.

[33] Fernando Ruiz Santiago, Pablo Tomás Muñoz, Elena Moya Sánchez, Marta Revelles Paniza, Alberto Martínez Martínez, and Antonio Luis Pérez Abela. Classifying thoracolumbar fractures: role of quantitative imaging. *Quantitative imaging in medicine and surgery*, 6(6):772, 2016.

[34] M Muratore, S Allasia, P Viglierchio, M Abbate, S Aleotti, A Masse, and A Bistolfi. Surgical treatment of traumatic thoracolumbar fractures: a retrospective review of 101 cases. *Musculoskeletal surgery*, pages 1–11, 2020.

[35] Y Hershkovitz, D Sheffer, K Peleg, Kessel Boris, JJ Dubose, I Jeroukhimov, A Givon, M Dudkiewicz, D Aranovich, et al. Thoracic vertebrae fracture: Is it an indicator of abdominal injury? *The American Journal of Emergency Medicine*, 2020.

[36] PAUL C McAfee, HA Yuan, BE Fredrickson, and JP Lubicky. The value of computed tomography in thoracolumbar fractures. *J Bone Joint Surg Am*, 65(4):461–473, 1983.

[37] Francis Denis. The three column spine and its significance in the classification of acute thoracolumbar spinal injuries. *spine*, 8(8):817–831, 1983.

[38] F Magerl, M Aebi, SD Gertzbein, J Harms, and S Nazarian. A comprehensive classification of thoracic and lumbar injuries. *European Spine Journal*, 3(4):184–201, 1994.

[39] Alexander R Vaccaro, Cumhur Oner, Christopher K Kepler, Marcel Dvorak, Klaus Schnake, Carlo Bellabarba, Max Reinhold, Bizhan Aarabi, Frank Kandziora, Jens Chapman, et al. Aospine thoracolumbar spine injury classification system: fracture description, neurological status, and key modifiers. *Spine*, 38(23):2028–2037, 2013.

[40] Tian-Xia Qiu, Kian-Wee Tan, Vee-Sin Lee, and Ee-Chon Teo. Investigation of thoracolumbar t12–l1 burst fracture mechanism using finite element method. *Medical engineering & physics*, 28(7):656–664, 2006.

[41] Robert F Heary and Sanjeev Kumar. Decision-making in burst fractures of the thoracolumbar and lumbar spine. *Indian journal of orthopaedics*, 41(4):268, 2007.

[42] Shaoyu Liu, Haomiao Li, Chunxiang Liang, Houqing Long, Binsheng Yu, Bailing Chen, Guowei Han, Xuhua Zhang, Fobao Li, and Fuxin Wei. Monosegmental transpedicular fixation for selected patients with thoracolumbar burst fractures. *Clinical Spine Surgery*, 22(1):38–44, 2009.

[43] Fu-Xin Wei, Shao-Yu Liu, Chun-Xiang Liang, Hao-Miao Li, Hou-Qing Long, Bin-Sheng Yu, Bai-Ling Chen, and Ke-Bing Chen. Transpedicular fixation in management of thoracolumbar burst fractures: monosegmental fixation versus short-segment instrumentation. *Spine*, 35(15):E714–E720, 2010.

[44] Ji wei Tian, Lei Wang, Tian Xia, Cheng yi Liu, Qing hua Zhao, and Shuang hai Dong. Posterior short-segmental fixation combined with intermediate screws vs conventional intersegmental fixation for monosegmental thoracolumbar fractures. *Orthopedics*, 34(8):e389–e396, 2011.

[45] Alex Vaccaro, Frank Kandziora, Michael Fehlings, and Rajasekaran Shanmughanathan. Posterior short segment fixation with intermediate screws. URL: `https://surgeryreference.aofoundation.org/spine/trauma/thoracolumbar/a4/posterior-short-segment-fixation-with-intermediate-screws`.

[46] Mauro Dobran, Davide Nasi, Denise Brunozzi, Lucia Di Somma, Maurizio Gladi, Maurizio Iacoangeli, and Massimo Scerrati. Treatment of unstable thoracolumbar junction fractures: short-segment pedicle fixation with inclusion of the fracture level versus long-segment instrumentation. *Acta neurochirurgica*, 158(10):1883–1889, 2016.

[47] Alex Vaccaro, Frank Kandziora, Michael Fehlings, and Rajasekaran Shanmughanathan. Posterior long segment fixation. URL: `https://surgeryreference.aofoundation.org/spine/trauma/thoracolumbar/a4/posterior-long-segment-fixation`.

[48] Alex Vaccaro, Frank Kandziora, Michael Fehlings, and Rajasekaran Shanmughanathan. Pedicle screw insertion. URL: `https://surgeryreference.aofoundation.org/spine/trauma/thoracolumbar/basic-technique/pedicle-screw-insertion`.

[49] Changxiang Liang, Guihua Liu, Guoyan Liang, Xiaoqing Zheng, Dong Yin, Dan Xiao, Shixing Zeng, Honghua Cai, and Yunbing Chang. Healing pattern classification for thoracolumbar burst fractures after posterior short-segment fixation. *BMC Musculoskeletal Disorders*, 21(1):1–10, 2020.

[50] Kelly Wade. Vertebral endplates. In *Biomechanics of the Spine*, pages 125–140. Elsevier, 2018.

[51] Chen-Sheng Chen, Cheng-Kung Cheng, Chien-Lin Liu, and Wai-Hee Lo. Stress analysis of the disc adjacent to interbody fusion in lumbar spine. *Medical engineering & physics*, 23(7):485–493, 2001.

[52] Francoise Marchand and Abdul M Ahmed. Investigation of the laminate structure of lumbar disc anulus fibrosus. *Spine*, 15(5):402–410, 1990.

[53] Sung M Moon, Jonathon H Yoder, Alexander C Wright, Lachlan J Smith, Edward J Vresilovic, and Dawn M Elliott. Evaluation of intervertebral disc cartilaginous endplate structure using magnetic resonance imaging. *European Spine Journal*, 22(8):1820–1828, 2013.

[54] VD Moramarco, A Pérez Del Palomar, C Pappalettere, and M Doblaré. An accurate validation of a computational model of a human lumbosacral segment. *Journal of biomechanics*, 43(2):334–342, 2010.

[55] Jason Tak-Man Cheung, Ming Zhang, and Daniel Hung-Kay Chow. Biomechanical responses of the intervertebral joints to static and vibrational loading: a finite element study. *Clinical Biomechanics*, 18(9):790–799, 2003.

[56] Grace D O'Connell, Heather L Guerin, and Dawn M Elliott. Theoretical and uniaxial experimental evaluation of human annulus fibrosus degeneration. *Journal of biomechanical engineering*, 131(11), 2009.

[57] M Dreischarf, T Zander, A Shirazi-Adl, CM Puttlitz, CJ Adam, CS Chen, VK Goel, A Kiapour, YH Kim, KM Labus, et al. Comparison of eight published static finite element models of the intact lumbar spine: predictive power of models improves when combined together. *Journal of biomechanics*, 47(8):1757–1766, 2014.

[58] Fang-Hsin Cheng, Shih-Liang Shih, Wen-Kai Chou, Chien-Lin Liu, Wen-Hsu Sung, and Chen-Sheng Chen. Finite element analysis of the scoliotic spine under different loading conditions. *Bio-medical materials and engineering*, 20(5):251–259, 2010.

[59] Pierre-Luc Sylvestre, Isabelle Villemure, and Carl-Eric Aubin. Finite element modeling of the growth plate in a detailed spine model. *Medical & biological engineering & computing*, 45(10):977–988, 2007.

[60] Hans de Visser, Clayton J Adam, Stuart Crozier, and Mark J Pearcy. The role of quadratus lumborum asymmetry in the occurrence of lesions in the lumbar vertebrae of cricket fast bowlers. *Medical engineering & physics*, 29(8):877–885, 2007.

[61] Taizo Hato, Norio Kawahara, Katsuro Tomita, Hideki Murakami, Tomoyuki Akamaru, Daisuke Tawara, Jiro Sakamoto, Juhachi Oda, and Shigenori Tanaka. Finite-element analysis on closing-opening correction osteotomy for angular kyphosis of osteoporotic vertebral fractures. *Journal of Orthopaedic Science*, 12(4):354–360, 2007.

[62] Wei Wang, Baoqing Pei, Yuyang Pei, Zhenpeng Shi, Chao Kong, Xueqing Wu, Nan Wu, Yubo Fan, and Shibao Lu. Biomechanical effects of posterior pedicle fixation techniques on the adjacent segment for the treatment of thoracolumbar burst fractures: a biomechanical analysis. *Computer methods in biomechanics and biomedical engineering*, 22(13):1083–1092, 2019.

[63] Toru Fujimoto, Akira Sei, Takuya Taniwaki, Tatsuya Okada, Toshitake Yakushiji, and Hiroshi Mizuta. Pedicle screw diameter selection for safe insertion in the thoracic spine. *European Journal of Orthopaedic Surgery & Traumatology*, 22(5):351–356, 2012.

[64] Alexander R Vaccaro, Steven J Rizzolo, Thomas J Allardyce, Matthew Ramsey, John Salvo, Richard A Balderston, and Jerome M Cotler. Placement of pedicle screws in the thoracic spine. part i: Morphometric analysis of the thoracic vertebrae. *The Journal of bone and joint surgery. American volume*, 77(8):1193–1199, 1995.

[65] Rohan-Jean Bianco, Pierre-Jean Arnoux, Jean-Marc Mac-Thiong, and Carl-Eric Aubin. Thoracic pedicle screw fixation under axial and perpendicular loadings: a comprehensive numerical analysis. *Clinical Biomechanics*, 68:190–196, 2019.

[66] Yongjung J Kim, Lawrence G Lenke, et al. Thoracic pedicle screw placement: free-hand technique. *Neurology India*, 53(4):512, 2005.

[67] Zhifeng Sun, Kaixiang Yang, Hongtao Chen, Tao Sui, Lei Yang, Dawei Ge, Jian Tang, and Xiaojian Cao. A novel entry point for pedicle screw placement in the thoracic spine. *Journal of biomedical research*, 32(2):123, 2018.

[68] Ronald A Lehman Jr, David W Polly Jr, Timothy R Kuklo, Bryan Cunningham, Kevin L Kirk, and Philip J Belmont Jr. Straight-forward versus anatomic trajectory technique of thoracic pedicle screw fixation: a biomechanical analysis. *Spine*, 28(18):2058–2065, 2003.

[69] Vernard S Fennell, Sheri Palejwala, Jesse Skoch, David A Stidd, and Ali A Baaj. Freehand thoracic pedicle screw technique using a uniform entry point and sagittal trajectory for all levels: preliminary clinical experience. *Journal of Neurosurgery: Spine*, 21(5):778–784, 2014.

[70] Dongsheng S Xu, Hao Wang, Jinhu H Zhang, Chunguang G Bai, and Rui Yang. Titanium alloys: from properties prediction to performance optimization. *Handbook of Materials Modeling: Applications: Current and Emerging Materials*, pages 113–151, 2020.

[71] Zhitao Xiao, Liya Wang, He Gong, and Dong Zhu. Biomechanical evaluation of three surgical scenarios of posterior lumbar interbody fusion by finite element analysis. *Biomedical engineering online*, 11(1):1–11, 2012.

[72] Etsuo Chosa, Keisuke Goto, Koji Totoribe, and Naoya Tajima. Analysis of the effect of lumbar spine fusion on the superior adjacent intervertebral disk in the presence of disk degeneration, using the three-dimensional finite element method. *Clinical Spine Surgery*, 17(2):134–139, 2004.

[73] ISAO Yamamoto, Manohar M Panjabi, TREY Crisco, and TOM Oxland. Three-dimensional movements of the whole lumbar spine and lumbosacral joint. *Spine*, 14(11):1256–1260, 1989.

[74] Thomas R Oxland, Ruey-Mo Lin, and Manohar M Panjabi. Three-dimensional mechanical properties of the thoracolumbar junction. *Journal of orthopaedic research*, 10(4):573–580, 1992.

[75] Marien Couvertier, Arnaud Germaneau, Mathieu Saget, Jean-Christophe Dupré, Pascal Doumalin, Fabrice Brémand, Franck Hesser, Cyril Brèque, Manuel Roulaud, Olivier Monlezun, et al. Biomechanical analysis of the thoracolumbar spine under physiological loadings: Experimental motion data corridors for validation of finite element models. *Proceedings of the Institution of Mechanical Engineers, Part H: Journal of Engineering in Medicine*, 231(10):975–981, 2017.

[76] Iris Busscher, Jaap H van Dieën, Albert J van der Veen, Idsart Kingma, Gerdine JM Meijer, Gijsbertus J Verkerke, and Albert G Veldhuizen. The effects of creep and recovery on the in vitro biomechanical characteristics of human multi-level thoracolumbar spinal segments. *Clinical biomechanics*, 26(5):438–444, 2011.